JIRBDAI

Journal of Institutional Research, Big Data Analytics and Innovation

Fractional-Order Modeling of Malaria Dynamics: A Mixed Fractional-Integer Model Approach for Epidemiological Analysis

Echude Ohiemi [1,2], Azuaba Emmanuel [2,3], M. O. Durojaye[2]

[1]Department of Mathematical Sciences, Veritas University Abuja, Nigeria,
[2]Department of Mathematics, Yakubu Gowon University, Abuja, Nigeria
[3]Department of Mathematical Sciences, Bingham University Karu, Nasarawa State, Nigeria
Corresponding Author: echudeo@veritas.edu.ng

ABSTRACT

Standard malaria models overlook how human immunity and healthcare decisions depend on past experiences (memory effect) and how random environmental fluctuations shape transmission. To address this, we developed a hybrid model: human infection dynamics use fractional-order calculus to capture memory, whereas mosquito dynamics remain integer-order but include environmental stochasticity. The analysis confirmed the existence, positivity, boundedness, and stability of the solution, with the basic reproduction number derived using next-generation methods. We solved the system using a fractional Adams–Bashforth–Moulton algorithm for humans and Euler–Maruyama for the stochastic mosquito component, calibrating the parameters with Nigeria's 2023 WHO malaria data and national surveys. Nigeria accounts for approximately 26–27% of global cases and 31% of deaths, making locally grounded models essential. Simulations show that stronger memory effects delay and lower epidemic peaks while prolonging the outbreaks. Critically, environmental randomness can drive disease extinction even when the deterministic reproduction number exceeds one. Incorporating both memory and stochasticity yields more realistic malaria dynamics and offers a refined framework for evaluating control strategies in high-burden settings.

KEYWORDS: Fractional Differential Equations; Caputo Derivative; Malaria Transmission; Stochastic Models; Mixed Integer-Fractional Models; Epidemiological Modeling; Numerical Simulation; Control Strategies

I. INTRODUCTION

Despite sustained control efforts, malaria remains one of the most persistent and devastating vector-borne diseases worldwide. The World Health Organization (WHO, 2023) reported 249 million cases and 608,000 deaths in 2022, with sub-Saharan Africa bearing 94% and 95% of this burden, respectively. Nigeria alone contributes approximately 27% of global cases, making locally grounded models essential. Large-scale interventions such as insecticide-treated nets (ITNs), indoor residual spraying (IRS), rapid diagnostic testing (RDT), and artemisinin combination therapies (ACTs) have curtailed malaria over the past two decades; however, progress has slowed recently due to insecticide and drug resistance, climate variability, and socioeconomic disparities (WHO, 2023). Mathematical modeling is indispensable for understanding malaria transmission, evaluating interventions, and informing public health decisions. Classical ordinary differential equation (ODE) models, beginning with the seminal Ross–Macdonald framework, have elucidated disease persistence, threshold phenomena, and host–vector interactions. However, these

Volume 2, Issue 3, 2026
https://doi.org/10.5281/zenodo.21990512

Markovian models assume that current disease dynamics depend only on the present state, neglecting the influence of past infections, acquired immunity, and treatment history. This omission is significant, as human immunity develops cumulatively over time, and individual behavior is shaped by prior experiences features that classical integer-order models cannot adequately capture (Diethelm, 2010; Podlubny, 1999). Fractional calculus has emerged as a powerful tool for modeling systems with memory and non-local interactions in biology. Fractional derivatives inherently incorporate the effect of previous states, making them well-suited for processes such as delayed immunity, long-lasting behavioral changes, and hereditary effects (Kilbas *et al*., 2006). Among fractional operators, the Caputo derivative is particularly attractive because it admits physically meaningful initial conditions and retains biological interpretability.

Recent malaria models employing fractional derivatives have demonstrated improved correspondence with disease dynamics. Abioye *et al*. (2023) examined a fractional-order co-infection model of malaria and COVID-19, showing that memory effects significantly influence disease persistence. Gizaw *et al*. (2024) incorporated climatic factors into a fractional malaria model for seasonal forecasting. Agbata *et al*. (2025a) used Caputo–Fabrizio and Atangana–Baleanu operators to study malaria transmission, while Jaleta *et al*. (2025) integrated treatment-seeking behavior into an Atangana–Baleanu fractional framework. Farman *et al*. (2025a, 2025b) analyzed fractal-fractional formulations, demonstrating greater flexibility than classical models.

Despite these advances, several limitations persist. First, most existing fractional models apply the same fractional operator identically to both human and mosquito populations, implicitly assuming equivalent memory properties in both groups an assumption lacking biological basis. Humans possess adaptive immune systems with memory lasting months to years, whereas mosquitoes have short lifespans (weeks) and no adaptive immunity. Second, many fractional models are purely deterministic, neglecting environmental stochasticity arising from climate variability, vector population fluctuations, and imperfect intervention implementation. Ignoring these factors can yield overly optimistic predictions of disease persistence or elimination. Third, few studies couple rigorous mathematical analysis with realistic numerical simulations calibrated to epidemiological data from endemic nations like Nigeria.

To address these gaps, we propose a hybrid malaria transmission model that combines Caputo fractional derivatives for human dynamics with classical integer-order differential equations for mosquito vectors, augmented by stochastic perturbations to capture environmental uncertainty. This framework achieves three novel integrations: (1) biologically appropriate memory effects in humans, (2) realistic vector dynamics without memory, and (3) environmental stochasticity features seldom considered together in a coherent formulation. The contributions of this study are fourfold. First, we develop a biologically consistent SEIRS–SEI malaria model that explicitly distinguishes the temporal properties of humans and mosquitoes. Second, we rigorously prove the existence, uniqueness, positivity, boundedness, and stability of solutions, establishing mathematical well-posedness. Third, we design an efficient numerical scheme combining the fractional Adams–Bashforth–Moulton predictor–corrector method with the Euler–Maruyama stochastic method for simulation. Finally, we calibrate the model using Nigerian malaria surveillance data and systematically investigate the effects of memory and environmental stochasticity on disease transmission, persistence, and elimination. Our findings provide novel insights into malaria dynamics and a robust framework to inform adaptive disease control strategies in endemic regions.

Volume 2, Issue 3, 2026
https://doi.org/10.5281/zenodo.21990512

Table 1: A Comprehensive Comparison Table and Expanded the Literature Review

Study	Fractional Operator	Stochasticity	Mixed-Order	Nigeria Calibration	Theoretical Analysis	Numerical Validation
Abioye et al. (2023)	Caputo	✗	✗	✗	✓	✓
Gizaw et al. (2024)	Caputo	✗	✗	✗	✓	✓
Agbata et al. (2025a)	CF, AB	✗	✗	✗	✓	✓
Jaleta et al. (2025)	ABC	✗	✗	✗	✓	✓
Farman et al. (2025a)	Fractal-fractional	✗	✗	✗	✓	✓
Farman et al. (2025b)	Fractal-fractional	✗	✗	✗	✓	✓
Abimbade et al. (2024)	Caputo	✗	✗	✓	✓	✓
Our Study	Caputo	✓	✓	✓	✓	

II. Model Formulation

A. Model Development and Biological Assumptions

Malaria is a vector-borne disease that requires the involvement of infected female Anopheles mosquitoes and susceptible humans. The biological dynamics of malaria transmission differ between human and mosquito populations. Partial immunity is built up over time in humans by exposure and past infections, and treatment history determines immune responses. Therefore, in human infection, the memory and hereditary properties of disease progression cannot be sufficiently captured by classical integer-order differential equations. In comparison, mosquitoes have relatively short life cycles and usually live for several weeks. The population dynamics of these species are sensitive to environmental factors such as rainfall, temperature, and availability of breeding habitat, and there is little sign of biological memory. Hence, classical first-order differential equations involving only integers should still be used to describe mosquito dynamics. Exploiting these biological disparities, we set up a combined fractional-integral-order malaria model. The Caputo fractional derivatives are employed to capture memory effects through immunity and disease processes for the human population, while ordinary differential equations are used to model the mosquito population. It is a hybrid model that embodies the features of fractional calculus, simplicity, and biological realism of classical epidemic models.

B. Biological Evidence for the Mixed-Order Approach

The immunological distinction between humans and mosquitoes is well-established in the literature. Humans develop adaptive immune responses to Plasmodium infection through multiple mechanisms:

(a). Persistence of acquired immunity: Studies have demonstrated that clinical immunity to malaria can persist for years, with antibody responses to certain antigens lasting 1-5 years following exposure (Rogerson et al., 2020; Crompton et al., 2014).

Volume 2, Issue 3, 2026
https://doi.org/10.5281/zenodo.21990512

(b). Immunological memory duration: Memory B cells and T cells specific to Plasmodium antigens have been detected up to 5-10 years post-infection (Langhorne et al., 2008; Ndungu et al., 2013). The gradual accumulation of immunity corresponds mathematically to fractional-order kinetics.

(c). Lack of adaptive immune memory in mosquitoes: Anopheles mosquitoes lack the adaptive immune system found in vertebrates and rely solely on innate immune responses. Their immune response to Plasmodium involves the Toll and Imd pathways but does not generate lasting immunological memory (Cirimotich et al., 2010; Blandin et al., 2008). With typical lifespans of 1-2 weeks in endemic regions, mosquito populations are governed by demographic processes rather than immunological memory.

The following assumptions were made for the model:

(a). There are four epidemiological classes: susceptible, exposed, infectious, and recovered.
(b). Infected mosquitoes spread the disease to susceptible humans after a good feed.
(c). Humans exposed to the virus remain in incubation for a period before they can infect others.
(d). People who are infected either recover or die due to malaria complications.
(e). Temporary immunity is lost over time, and the recovered individual moves back to the susceptible class.
(f). The mosquito population was segmented into susceptible, exposed, and infectious populations.
(g). Mosquitoes can be infected by feeding on infected humans.
(h). Malaria parasites are not naturally cleared from mosquitoes, and once infected, the mosquito will continue to be infectious until death.
(i). Human demographic processes have memory effects and are described by Caputo fractional derivatives of order $0 < \alpha \leq 1$, whereas mosquito dynamics are described by classical integer-order equations.
(j). Stochastic perturbations represent environmental uncertainty caused by climate variability, vector control activities, and ecological fluctuations.

These assumptions enable a biologically consistent approach to the study of malaria transmission and the different temporal patterns of human and mosquito populations.

C. Mathematical Preliminaries

Throughout this work, let $0 < \alpha \leq 1$, where α denotes the fractional order of differentiation. Let

$$C([0,T],\mathbb{R}^n) \quad (1)$$

be the Banach space of continuous vector-valued functions defined on the interval $[0, T]$, equipped with the supremum norm

$$\|x\|_\infty = \max_{0\leq t\leq T} |x(t)|. \quad (2)$$

The Caputo fractional derivative is adopted because it allows the use of classical initial conditions and has become one of the most widely used operators in biological and epidemiological modelling.

(a). Definition 2.1 (Caputo Fractional Derivative)

Let $x(t)$ be continuously differentiable on $[0, T]$. The Caputo fractional derivative of order $0 < \alpha < 1$ is defined by

Volume 2, Issue 3, 2026
https://doi.org/10.5281/zenodo.21990512

$$ {}^{C}D_t^{\alpha} x(t) = \frac{1}{\Gamma(1-\alpha)} \int_0^t \frac{x'(s)}{(t-s)^{\alpha}} ds, \quad (3) $$

where $\Gamma(\cdot)$ denotes the Gamma function. Unlike ordinary differentiation, the Caputo operator depends on the entire history of the solution. Consequently, the current disease dynamics are influenced not only by the present state of the system but also by previous exposure and immune responses.

(b). Definition 2.2 (Mittag–Leffler Function)
The Mittag–Leffler function is defined by:

$$ E_{\alpha}(z) = \sum_{k=0}^{\infty} \frac{z^k}{\Gamma(\alpha k + 1)}, \alpha > 0. \quad (4) $$

This function generalizes the exponential function and naturally appears in the solutions of linear fractional differential equations.

D. Model Variables

The total human population is denoted by:

$$ N_h(t) = S_h(t) + E_h(t) + I_h(t) + R_h(t), \quad (5) $$

where $S_h(t)$denotes susceptible humans, $E_h(t)$denotes exposed humans, $I_h(t)$denotes infectious humans, $R_h(t)$denotes recovered humans. Similarly, the mosquito population is

$$ N_m(t) = S_m(t) + E_m(t) + I_m(t), \quad (6) $$

where $S_m(t)$represents susceptible mosquitoes, $E_m(t)$represents exposed mosquitoes, $I_m(t)$represents infectious mosquitoes. The force of infection from mosquitoes to humans is assumed to be $\lambda_h = \beta_{hm} I_m$, whereas the force of infection from humans to mosquitoes is $\lambda_m = \beta_{mh} I_h$. Here, β_{hm} and β_{mh}; represent the effective transmission rates from mosquitoes to humans and from humans to mosquitoes, respectively.

Table 2: Model Parameters and Biological Interpretations

Parameter	Biological Meaning	Units
$\boldsymbol{\Lambda_h}$	Human recruitment rate	humans/day
$\boldsymbol{\Lambda_m}$	Mosquito recruitment rate	mosquitoes/day
$\boldsymbol{\beta_{hm}}$	Human infection rate from mosquitoes	1/(mosquito·day)
$\boldsymbol{\beta_{mh}}$	Mosquito infection rate from humans	1/(human·day)
$\boldsymbol{\mu_h}$	Human natural mortality rate	1/day
$\boldsymbol{\mu_m}$	Mosquito mortality rate	1/day
$\boldsymbol{\sigma_h}$	Human latent to infectious rate	1/day
$\boldsymbol{\sigma_m}$	Mosquito latent to infectious rate	1/day
$\boldsymbol{\gamma_h}$	Human recovery rate	1/day
$\boldsymbol{\delta_h}$	Disease-induced mortality in humans	1/day

Volume 2, Issue 3, 2026
https://doi.org/10.5281/zenodo.21990512

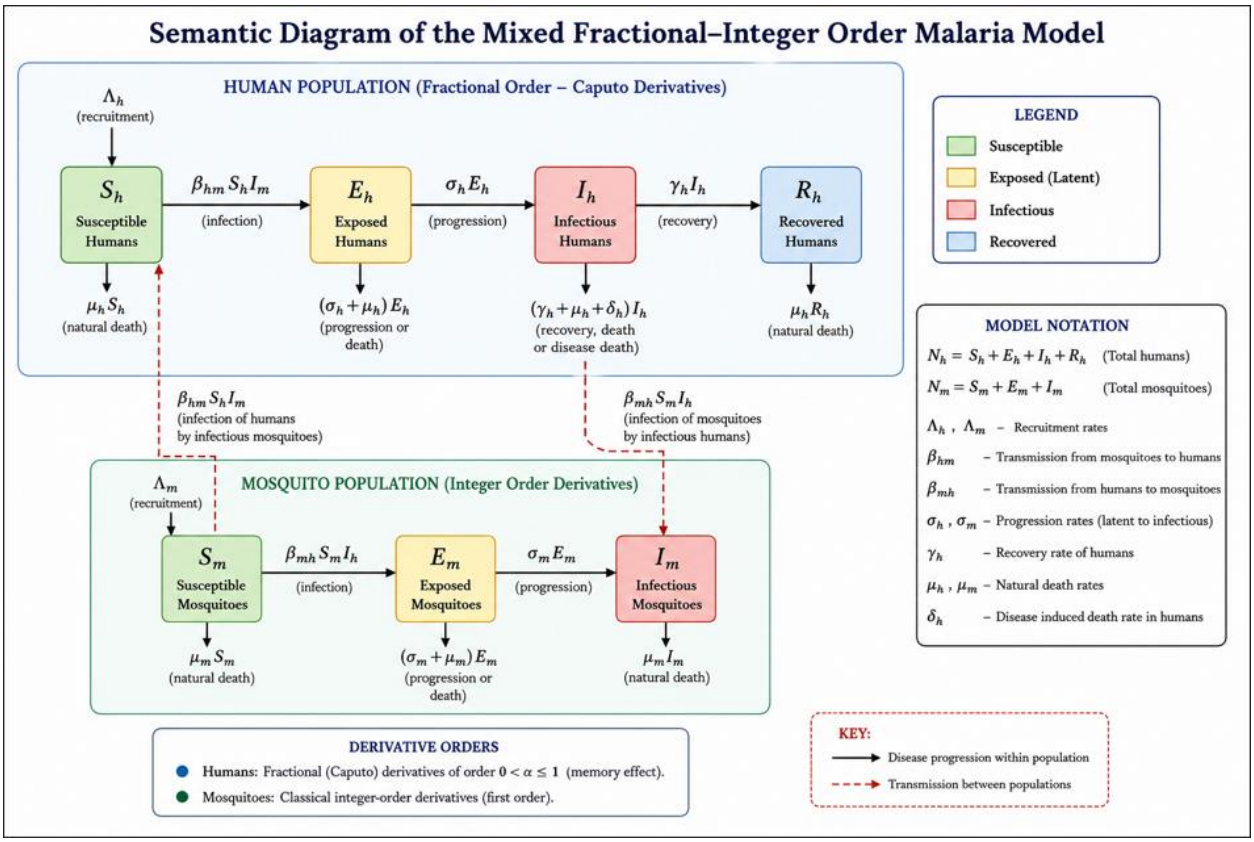

Figure 1: Flowchart of the mixed Fractional Order Malaria Model

E. Mixed Fractional–Integer Malaria Model

Using the biological assumptions described above, the transmission dynamics are governed by the following coupled systems:

(a). Human population (fractional dynamics)

$$^{C}D_t^{\alpha} S_h = \Lambda_h - \beta_{hm} S_h I_m - \mu_h S_h + \rho R_h, \quad (7)$$

$$^{C}D_t^{\alpha} E_h = \beta_{hm} S_h I_m - (\sigma_h + \mu_h) E_h, \quad (8)$$

$$^{C}D_t^{\alpha} I_h = \sigma_h E_h - (\gamma_h + \delta_h + \mu_h) I_h, \quad (9)$$

$$^{C}D_t^{\alpha} R_h = \gamma_h I_h - (\rho + \mu_h) R_h. \quad (10)$$

The fractional derivative reflects the cumulative influence of previous infections and immune responses on human population evolution.

(b). Mosquito population (integer dynamics)

The mosquito population evolves according to

$$\frac{dS_m}{dt} = \Lambda_m - \beta_{mh} S_m I_h - \mu_m S_m, \quad (11)$$

$$\frac{dE_m}{dt} = \beta_{mh} S_m I_h - (\sigma_m + \mu_m) E_m, \quad (12)$$

$$\frac{dI_m}{dt} = \sigma_m E_m - \mu_m I_m. \quad (13)$$

Unlike humans, mosquitoes have relatively short lifespans and do not develop adaptive immunity. Consequently, their dynamics are adequately described by ordinary differential equations, without

Volume 2, Issue 3, 2026
https://doi.org/10.5281/zenodo.21990512

memory effects. Therefore, the complete system combines fractional dynamics for the human host with classical integer-order dynamics for the mosquito vector. This hybrid structure captures the long-term memory associated with human immunity while preserving the rapid biological processes governing mosquito populations.

F. Biological Interpretation of the Fractional Order

Mosquitoes are not mammals; they have a short lifespan and lack adaptive immunity. This makes the dynamics of these two well described by ordinary differential equations in which there are no memory effects. The overall dynamics are thus mixed because the human host is modelled with fractional dynamics and the mosquito with classical integer-order dynamics. This combination has the biological processes of mosquito populations and the long-term memory of human immunity. In addition to the above, the fractional order is biological in nature. In addition to the above, the fractional order is also biological. The number α determines the degree of memory in human society, and $\alpha = 0,$ indicates that there is no memory. The proposed model is reduced to the classical malaria model with integer order as $\alpha = 1$, which assumes that disease transmission depends only on the current epidemiological status. The system has memory for $0 < \alpha < 1$, that is, the disease progression is influenced by the past records of disease exposure. Historical data have a greater impact on their dynamics as the fractional order decreases, resulting in slower epidemic dynamics, longer infectious periods, and slower convergence to equilibrium. These properties are similar to malaria epidemiology in the field, where natural immunity is acquired over time with repeated exposure and decays with time. Therefore, the mixed fractional formulation represents a biologically realistic malaria transmission model that is mathematically tractable for theoretical analysis and numerical simulation.

G. Stochastic Extension

To capture environmental stochasticity, such as weather variations and irregular intervention implementation, we incorporated multiplicative noise terms

For human compartments:

$$ {}^{C}D_t^{\alpha} X_h(t) = f_X\big(X_h(t), X_m(t)\big) + \sigma_{X_h} X_h(t) \cdot \dot{W}_{X_h}(t), \tag{14}$$

and for mosquito compartments:

$$ dY_m(t) = g_Y\big(X_h(t), Y_m(t)\big)\, dt + \sigma_{Y_m} Y_m(t)\, dW_{Y_m}(t), \tag{15}$$

where W(t) is an independent standard Wiener process and σ is the noise intensity. The multiplicative form ensures that the noise magnitude scales with the population size, preserving biological realism.

III. MATHEMATICAL ANALYSIS

Existence and Uniqueness of Solutions

We consider the initial value problem for the fractional subsystem (7) - (10) in this section. Let the state vector be:

$$\mathbf{X}(t) = (S_h(t), E_h(t), I_h(t), R_h(t))^T \in \mathbb{R}_+^4,$$

and define the vector field by $\mathbf{F}: [0,T] \times \mathbb{R}_+^4 \to \mathbb{R}^4$ by

$$\mathbf{F}(t, \mathbf{X}) = \begin{pmatrix} \Lambda_h - \beta_{hm} S_h I_m - \mu_h S_h \\ \beta_{hm} S_h I_m - (\sigma_h + \mu_h) E_h \\ \sigma_h E_h - (\gamma_h + \mu_h + \delta_h) I_h \\ \gamma_h I_h - \mu_h R_h \end{pmatrix}. \tag{16}$$

Volume 2, Issue 3, 2026
https://doi.org/10.5281/zenodo.21990512

The fractional system can then be written compactly as:

$$^{C}D_t^{\alpha}\mathrm{X}(t) = \mathrm{F}(t,\mathrm{X}(t)), t \in [0,T], \mathrm{X}(0) = \mathrm{X}_0 \in \mathbb{R}_+^4. \quad (17)$$

Theorem 1: Existence and Uniqueness

Let $\alpha \in (0,1]$, $T > 0$, and $\mathrm{X}_0 \in \mathbb{R}_+^4$. Suppose F: $[0,T] \times \mathbb{R}^4 \to \mathbb{R}^4$is continuous in $t$and satisfies a Lipschitz condition in X: there exists $L > 0$such that:

$$\|\mathrm{F}(t,\mathrm{X}_1) - \mathrm{F}(t,\mathrm{X}_2)\| \le L\|\mathrm{X}_1 - \mathrm{X}_2\| \quad (18)$$

for all $t \in [0,T]$and $\mathrm{X}_1, \mathrm{X}_2 \in \mathbb{R}^4$. Then the initial value problem (17) admits a unique solution $\mathrm{X} \in C([0,T],\mathbb{R}^4)$.

Proof.

By the fundamental theorem of fractional calculus, the Caputo fractional initial value problem (17) is equivalent to the Volterra integral equation:

$$\mathrm{X}(t) = \mathrm{X}_0 + \frac{1}{\Gamma(\alpha)}\int_0^t (t-s)^{\alpha-1}\,\mathrm{F}(s,\mathrm{X}(s))\,ds. \quad (19)$$

Define the operator $\mathcal{T}: C([0,T],\mathbb{R}^4) \to C([0,T],\mathbb{R}^4)$by

$$(\mathcal{T}\mathrm{X})(t) = \mathrm{X}_0 + \frac{1}{\Gamma(\alpha)}\int_0^t (t-s)^{\alpha-1}\,\mathrm{F}(s,\mathrm{X}(s))\,ds. \quad (20)$$

For any $\mathrm{X}, \mathrm{Y} \in C([0,T],\mathbb{R}^4)$, we obtain

$$\|(\mathcal{T}\mathrm{X})(t) - (\mathcal{T}\mathrm{Y})(t)\| \le \frac{1}{\Gamma(\alpha)}\int_0^t (t-s)^{\alpha-1}\|\mathrm{F}(s,\mathrm{X}(s)) - \mathrm{F}(s,\mathrm{Y}(s))\|ds. \quad (21)$$

Using the Lipschitz condition (18) gives

$$\|(\mathcal{T}\mathrm{X})(t) - (\mathcal{T}\mathrm{Y})(t)\| \le \frac{L}{\Gamma(\alpha)}\int_0^t (t-s)^{\alpha-1}\|\mathrm{X}(s) - \mathrm{Y}(s)\|ds. \quad (22)$$

Taking the supremum over $t \in [0,T]$gives

$$\| \mathcal{T}\mathrm{X} - \mathcal{T}\mathrm{Y} \|_{\infty} \le \frac{LT^{\alpha}}{\Gamma(\alpha+1)} \| \mathrm{X} - \mathrm{Y} \|_{\infty}. \quad (23)$$

Define $\delta = \frac{LT^{\alpha}}{\Gamma(\alpha+1)}$. For Tsufficiently small so that $\delta < 1$, the operator $\mathcal{T}$is a contraction on the complete metric space $C([0,T],\mathbb{R}^4)$. By Banach's fixed-point theorem, $\mathcal{T}$has a unique fixed point, which is the unique solution of (144) and therefore of (17). To extend the solution to arbitrary Twe use a continuation argument. Let T^*be the supremum of all $T$for which a unique solution exists. If $T^* < \infty$, the contraction argument above allows extension of the solution beyond T^*, contradicting the maximality of T^*. Hence $T^* = \infty$ and the solution exists globally.

Positivity and Biological Feasibility

Theorem 2: Positivity

Let $\mathbf{X}(0) \ge 0$ component wise. Then the solution $\mathbf{X}(t)$of system (17) satisfies $\mathbf{X}(t) \ge 0$for all $t \ge 0$.

Proof. We use the generalized mean value theorem for fractional derivatives. For $0 < \alpha < 1$, if $f \in C[0,T]$and $^{C}D_t^{\alpha} f \in C(0,T]$, then for any $t \in (0,T]$,

$$f(t) = f(0) + \frac{1}{\Gamma(\alpha)}\int_0^t (t-s)^{\alpha-1}\,{}^{C}D_s^{\alpha} f(s)\,ds. \quad (24)$$

Volume 2, Issue 3, 2026
https://doi.org/10.5281/zenodo.21990512

Examine each compartment on the boundary of the non-negative orthant. Suppose $S_h(t^*)$attains its first zero at some $t^* > 0$, with all other compartments non-negative. Then at this point

$$^{C}D_t^{\alpha} S_h(t^*) = \Lambda_h + \beta_{hm} S_h(t^*) I_m(t^*) - \mu_h S_h(t^*) = \Lambda_h > 0. \quad (25)$$

By the generalized mean value theorem, $S_h(t)$increases immediately after t^*, contradicting that $S_h$first reached zero there. Thus $S_h(t) \geq 0$for all t. Similar arguments apply to the other compartments. For E_h, at the boundary $E_h(t^*) = 0$,

$$^{C}D_t^{\alpha} E_h(t^*) = \beta_{hm} S_h(t^*) I_m(t^*) \geq 0. \quad (26)$$

For I_h, at $I_h(t^*) = 0$,

$$^{C}D_t^{\alpha} I_h(t^*) = \sigma_h E_h(t^*) \geq 0. \quad (27)$$

For R_h, at $R_h(t^*) = 0$,

$$^{C}D_t^{\alpha} R_h(t^*) = \gamma_h I_h(t^*) \geq 0. \quad (28)$$

Therefore, all solutions remain non-negative for all $t \geq 0$.

Theorem 3: Invariant Region

The set

$$\Omega = \left\{(S_h, E_h, I_h, R_h, S_m, E_m, I_m) \in \mathbb{R}_+^7 : N_h \leq \frac{\Lambda_h}{\mu_h},\ N_m \leq \frac{\Lambda_m}{\mu_m}\right\} \quad (29)$$

is positively invariant for system (7) – (13).

Proof. For the total human population $N_h = S_h + E_h + I_h + R_h$, summing equations (7) - (10) and using linearity of the fractional derivative gives

$$^{C}D_t^{\alpha} N_h(t) = \Lambda_h - \mu_h N_h(t) - \delta_h I_h(t) \leq \Lambda_h - \mu_h N_h(t). \quad (30)$$

By the fractional comparison principle,

$$N_h(t) \leq N_h(0) E_{\alpha,1}(-\mu_h t^{\alpha}) + \frac{\Lambda_h}{\mu_h}[1 - E_{\alpha,1}(-\mu_h t^{\alpha})], \quad (31)$$

where $E_{\alpha,1}$is the Mittag–Leffler function. Since $E_{\alpha,1}(-\mu_h t^{\alpha}) \to 0$as $t \to \infty$,

$$\limsup_{t\to\infty} N_h(t) \leq \frac{\Lambda_h}{\mu_h}. \quad (32)$$

For the mosquito population $N_m = S_m + E_m + I_m$, summing (11) - (13) yields the ODE

$$\dot{N}_m(t) = \Lambda_m - \mu_m N_m(t). \quad (33)$$

Its solution is

$$N_m(t) = N_m(0) e^{-\mu_m t} + \frac{\Lambda_m}{\mu_m}(1 - e^{-\mu_m t}). \quad (34)$$

Hence $\limsup_{t\to\infty} N_m(t) \leq \Lambda_m/\mu_m$, and therefore $\Omega$is positively invariant.

Theorem 4: Boundedness

All solutions of system (7) - (13) with non-negative initial conditions are uniformly bounded.

Proof: The boundedness follows directly from Theorem 3.3. Since Ω is positively invariant and contains all non-negative initial conditions, every trajectory remains within the compact set $\bar{\Omega}$. In particular, each compartment satisfies the following bounds:

$$0 \leq S_h(t), E_h(t), I_h(t), R_h(t) \leq \frac{\Lambda_h}{\mu_h}, \quad (35)$$

Volume 2, Issue 3, 2026
https://doi.org/10.5281/zenodo.21990512

$$0 \le S_m(t), E_m(t), I_m(t) \le \frac{\Lambda_m}{\mu_m}. \quad (36)$$

These bounds are uniform in t and depend only on the model parameters.

B. Disease-Free Equilibrium

(a). Existence and Computation

The Disease-Free Equilibrium (DFE) is obtained by setting all infected compartments to zero and solving the resulting algebraic system. For the fractional subsystem (7) - (10) at equilibrium, we have ${}^{C}D_t^{\alpha} X = 0$ for each compartment X, which yields

$$0 = \Lambda_h - \beta_{hm} S_h^0 I_m^0 - \mu_h S_h^0, \quad (37)$$
$$0 = \beta_{hm} S_h^0 I_m^0 - (\sigma_h + \mu_h) E_h^0, \quad (38)$$
$$0 = \sigma_h E_h^0 - (\gamma_h + \mu_h + \delta_h) I_h^0, \quad (39)$$
$$0 = \gamma_h I_h^0 - \mu_h R_h^0. \quad (3.25)$$

At the DFE, $E_h^0 = I_h^0 = R_h^0 = 0$and $I_m^0 = 0$. Substituting into (37) gives

$$0 = \Lambda_h - \mu_h S_h^0 \implies S_h^0 = \frac{\Lambda_h}{\mu_h}. \quad (40)$$

Similarly, for the mosquito subsystem at equilibrium with $E_m^0 = I_m^0 = 0$, we obtain

$$0 = \Lambda_m - \mu_m S_m^0 \implies S_m^0 = \frac{\Lambda_m}{\mu_m}. \quad (41)$$

Thus, the DFE is explicitly given by

$$E_0 = \left(\frac{\Lambda_h}{\mu_h}, 0, 0, 0, \frac{\Lambda_m}{\mu_m}, 0, 0\right). \quad (42)$$

(b). Biological Interpretation

The DFE represents a state where malaria is absent from the population. All humans are susceptible ($S_h = \Lambda_h/\mu_h$), which is the equilibrium susceptible population in the absence of infection. Similarly, all mosquitoes are susceptible ($S_m = \Lambda_m/\mu_m$). This state is maintained solely by the balance between recruitment and natural mortality in both populations. Biological significance: the DFE is a threshold state. If the disease is introduced at the DFE and the basic reproduction number $R_0 < 1$, the infection will die out and the system returns to the DFE. If $R_0 > 1$, the DFE is unstable and the disease will establish itself, leading to an endemic equilibrium.

(c). Basic Reproduction Number

We compute R_0using the next-generation matrix approach. Let $\mathbf{x} = (E_h, I_h, E_m, I_m)^T$be the vector of infected compartments. The infected subsystem can be written as

$${}^{C}D_t^{\alpha}\mathbf{x} = \mathcal{F}(\mathbf{x}) - \mathcal{V}(\mathbf{x}), \quad (43)$$

where $\mathcal{F}$represents new infections entering each compartment and $\mathcal{V}$ represents transfer out of each compartment. From system (1) - (7),

$$\mathcal{F}(\mathbf{x}) = \begin{pmatrix} \beta_{hm} S_h I_m \\ 0 \\ \beta_{mh} S_m I_h \\ 0 \end{pmatrix}, \quad (44)$$

Volume 2, Issue 3, 2026
https://doi.org/10.5281/zenodo.21990512

$$\mathcal{V}(\mathbf{x}) = \begin{pmatrix} (\sigma_h + \mu_h)E_h \\ -\sigma_h E_h + (\gamma_h + \mu_h + \delta_h)I_h \\ (\sigma_m + \mu_m)E_m \\ -\sigma_m E_m + \mu_m I_m \end{pmatrix}. \quad (45)$$

At the DFE, $S_h^0 = \Lambda_h/\mu_h$ and $S_m^0 = \Lambda_m/\mu_m$. The Jacobian matrices of $\mathcal{F}$ and $\mathcal{V}$ at the DFE are:

$$F = \begin{pmatrix} 0 & 0 & 0 & \beta_{hm}\Lambda_h/\mu_h \\ 0 & 0 & 0 & 0 \\ 0 & \beta_{mh}\Lambda_m/\mu_m & 0 & 0 \\ 0 & 0 & 0 & 0 \end{pmatrix}, \quad (46)$$

$$V = \begin{pmatrix} \sigma_h + \mu_h & 0 & 0 & 0 \\ -\sigma_h & \gamma_h + \mu_h + \delta_h & 0 & 0 \\ 0 & 0 & \sigma_m + \mu_m & 0 \\ 0 & 0 & -\sigma_m & \mu_m \end{pmatrix}. \quad (47)$$

The inverse of V is

$$V^{-1} = \begin{pmatrix} \frac{1}{\sigma_h + \mu_h} & 0 & 0 & 0 \\ \frac{\sigma_h}{(\sigma_h + \mu_h)(\gamma_h + \mu_h + \delta_h)} & \frac{1}{\gamma_h + \mu_h + \delta_h} & 0 & 0 \\ 0 & 0 & \frac{1}{\sigma_m + \mu_m} & 0 \\ 0 & 0 & \frac{\sigma_m}{(\sigma_m + \mu_m)\mu_m} & \frac{1}{\mu_m} \end{pmatrix}. \quad (48)$$

The next-generation matrix is $K = FV^{-1}$. Computing K explicitly gives

$$K = \begin{pmatrix} 0 & 0 & \frac{\beta_{hm}\Lambda_h\sigma_m}{\mu_h(\sigma_m + \mu_m)\mu_m} & \frac{\beta_{hm}\Lambda_h}{\mu_h\mu_m} \\ 0 & 0 & 0 & 0 \\ \frac{\beta_{mh}\Lambda_m\sigma_h}{\mu_m(\sigma_h + \mu_h)(\gamma_h + \mu_h + \delta_h)} & \frac{\beta_{mh}\Lambda_m}{\mu_m(\gamma_h + \mu_h + \delta_h)} & 0 & 0 \\ 0 & 0 & 0 & 0 \end{pmatrix}. \quad (49)$$

The basic reproduction number R_0 is the spectral radius of K:

$$R_0 = \rho(K).$$

Since K has block structure, the non-zero eigenvalues satisfy

$$\lambda^2 = \frac{\beta_{hm}\Lambda_h}{\mu_h} \cdot \frac{\sigma_m}{(\sigma_m + \mu_m)\mu_m} \cdot \frac{\beta_{mh}\Lambda_m}{\mu_m} \cdot \frac{\sigma_h}{(\sigma_h + \mu_h)(\gamma_h + \mu_h + \delta_h)}. \quad (50)$$

Therefore,

$$R_0 = \sqrt{\frac{\beta_{hm}\beta_{mh}\Lambda_h\Lambda_m\sigma_h\sigma_m}{\mu_h\mu_m^2(\sigma_h + \mu_h)(\gamma_h + \mu_h + \delta_h)(\sigma_m + \mu_m)\mu_m}}. \quad (51)$$

Alternatively,

$$R_0 = \sqrt{R_{hm} \cdot R_{mh}}, \quad (52)$$

where:

$$R_{hm} = \frac{\beta_{hm}\Lambda_h}{\mu_h} \cdot \frac{\sigma_m}{(\sigma_m + \mu_m)\mu_m} \quad (53)$$

Volume 2, Issue 3, 2026
https://doi.org/10.5281/zenodo.21990512

is the number of secondary human infections generated by one infected mosquito, and

$$R_{mh} = \frac{\beta_{mh}\Lambda_m}{\mu_m} \cdot \frac{\sigma_h}{(\sigma_h + \mu_h)(\gamma_h + \mu_h + \delta_h)} \tag{54}$$

is the number of secondary mosquito infections generated by one infected human.

(d). Biological Interpretation of R_0

The expression for R_0 has a clear epidemiological interpretation:

(a). Human-to-mosquito transmission component:

i. β_{mh}: rate at which susceptible mosquitoes become infected by infectious humans
ii. Λ_m/μ_m: equilibrium susceptible mosquito population
iii. $\sigma_h/(\sigma_h + \mu_h)$: probability an exposed human survives the latent period to become infectious
iv. $1/(\gamma_h + \mu_h + \delta_h)$: average duration of human infectiousness

(b). Mosquito-to-human transmission component:

i. β_{hm}: rate at which susceptible humans become infected by infectious mosquitoes
ii. Λ_h/μ_h: equilibrium susceptible human population
iii. $\sigma_m/(\sigma_m + \mu_m)$: probability an exposed mosquito survives the sporogonic cycle to become infectious
iv. $1/\mu_m$: average lifespan of an infectious mosquito

The square root arises because malaria transmission requires two sequential infection events: human → mosquito → human. Thus, R_0 is the geometric mean of the number of human infections per mosquito infection and the number of mosquito infections per human infection.

C. Endemic Equilibrium

(a). Derivation and Existence

Let $E^* = (S_h^*, E_h^*, I_h^*, R_h^*, S_m^*, E_m^*, I_m^*)$ denote the endemic equilibrium, where all infected compartments are positive. At equilibrium, the fractional derivatives vanish. From equations (7) - (13) we obtain:

$$\Lambda_h - \beta_{hm} S_h^* I_m^* - \mu_h S_h^* = 0, \tag{55}$$
$$\beta_{hm} S_h^* I_m^* - (\sigma_h + \mu_h) E_h^* = 0, \tag{56}$$
$$\sigma_h E_h^* - (\gamma_h + \mu_h + \delta_h) I_h^* = 0, \tag{57}$$
$$\gamma_h I_h^* - \mu_h R_h^* = 0, \tag{58}$$
$$\Lambda_m - \beta_{mh} S_m^* I_h^* - \mu_m S_m^* = 0, \tag{59}$$
$$\beta_{mh} S_m^* I_h^* - (\sigma_m + \mu_m) E_m^* = 0, \tag{60}$$
$$\sigma_m E_m^* - \mu_m I_m^* = 0. \tag{61}$$

From (57),

$$E_h^* = \frac{\gamma_h + \mu_h + \delta_h}{\sigma_h} I_h^*. \tag{62}$$

From (56),

$$S_h^* = \frac{(\sigma_h + \mu_h) E_h^*}{\beta_{hm} I_m^*} = \frac{(\sigma_h + \mu_h)(\gamma_h + \mu_h + \delta_h)}{\beta_{hm}\sigma_h} \cdot \frac{I_h^*}{I_m^*}. \tag{63}$$

From (55),

$$\Lambda_h = \mu_h S_h^* + \beta_{hm} S_h^* I_m^*. \tag{64}$$

Volume 2, Issue 3, 2026
https://doi.org/10.5281/zenodo.21990512

Substituting (64) into (65) yields

$$\Lambda_h = \frac{(\sigma_h + \mu_h)(\gamma_h + \mu_h + \delta_h)}{\beta_{hm}\sigma_h} \cdot \frac{I_h^*}{I_m^*}(\mu_h + \beta_{hm} I_m^*). \tag{65}$$

Similarly, from the mosquito equations:

$$E_m^* = \frac{\mu_m}{\sigma_m} I_m^*, \tag{66}$$

$$S_m^* = \frac{(\sigma_m + \mu_m)E_m^*}{\beta_{mh} I_h^*} = \frac{(\sigma_m + \mu_m)\mu_m}{\beta_{mh}\sigma_m} \cdot \frac{I_m^*}{I_h^*}, \tag{67}$$

and from (59),

$$\Lambda_m = \mu_m S_m^* + \beta_{mh} S_m^* I_h^*. \tag{68}$$

Substituting (67) into (68):

$$\Lambda_m = \frac{(\sigma_m + \mu_m)\mu_m}{\beta_{mh}\sigma_m} \cdot \frac{I_m^*}{I_h^*}(\mu_m + \beta_{mh} I_h^*). \tag{69}$$

Let $x = I_h^*$ and $y = I_m^*$. From (65) and (69) we obtain a system of two algebraic equations. Multiplying (65) and (69) yields

$$\Lambda_h \Lambda_m = \frac{(\sigma_h + \mu_h)(\gamma_h + \mu_h + \delta_h)(\sigma_m + \mu_m)\mu_m}{\beta_{hm}\beta_{mh}\sigma_h\sigma_m} \cdot (\mu_h + \beta_{hm} y)(\mu_m + \beta_{mh} x). \tag{70}$$

Using the definition of R_0 from (51), we can rewrite this as

$$R_0^2 = \frac{\mu_h \mu_m}{\Lambda_h \Lambda_m} \cdot \frac{(\sigma_h + \mu_h)(\gamma_h + \mu_h + \delta_h)(\sigma_m + \mu_m)\mu_m}{\beta_{hm}\beta_{mh}\sigma_h\sigma_m} \cdot \Lambda_h \Lambda_m. \tag{71}$$

Substituting into (3.57):

$$\frac{\Lambda_h \Lambda_m}{\mu_h \mu_m} R_0^2 = \frac{\Lambda_h \Lambda_m}{\mu_h \mu_m}\left(1 + \frac{\beta_{hm} y}{\mu_h}\right)\left(1 + \frac{\beta_{mh} x}{\mu_m}\right). \tag{72}$$

Thus,

$$R_0^2 = \left(1 + \frac{\beta_{hm} I_m^*}{\mu_h}\right)\left(1 + \frac{\beta_{mh} I_h^*}{\mu_m}\right). \tag{73}$$

From (70), solve for I_m^* in terms of I_h^*:

$$I_m^* = \frac{\mu_h \sigma_h \Lambda_h I_h^*}{\beta_{hm}(\sigma_h + \mu_h)(\gamma_h + \mu_h + \delta_h) I_h^* - \mu_h \sigma_h \Lambda_h}. \tag{74}$$

Substituting this into (73) yields a polynomial in I_h^*. The endemic equilibrium exists if and only if this polynomial has a positive real root, which occurs precisely when $R_0 > 1$.

(b). Existence Condition

Theorem 5: Existence of Endemic Equilibrium

The system (7) - (13) has a unique endemic equilibrium E^* with all infected components positive if and only if $R_0 > 1$.

Proof: From (73), for $I_h^* > 0$ and $I_m^* > 0$ we must have

$$R_0^2 > 1 \iff R_0 > 1. \tag{75}$$

Conversely, if $R_0 > 1$, we can solve for I_h^* explicitly. Let

$$A = \frac{(\sigma_h + \mu_h)(\gamma_h + \mu_h + \delta_h)}{\sigma_h} > 0, \tag{76}$$

$$B = \frac{(\sigma_m + \mu_m)\mu_m}{\sigma_m} > 0. \tag{77}$$

Volume 2, Issue 3, 2026
https://doi.org/10.5281/zenodo.21990512

Then from (63) and 67),

$$S_h^* = \frac{A}{\beta_{hm}} \cdot \frac{I_h^*}{I_m^*}, S_m^* = \frac{B}{\beta_{mh}} \cdot \frac{I_m^*}{I_h^*}. \quad (78)$$

Substituting into the equilibrium equations gives a quadratic in I_h^*:

$$(R_0^2 - 1)I_h^* = \frac{\mu_m}{\beta_{mh}}(R_0^2 - 1)\frac{\Lambda_h}{\mu_h} + \frac{\beta_{hm}}{\mu_h}\left(\frac{\mu_m}{\beta_{mh}}\right)^2 \frac{\Lambda_h}{\mu_h} I_h^*. \quad (79)$$

This yields

$$I_h^* = \frac{\mu_m}{\beta_{mh}} \frac{R_0^2 - 1}{R_0^2 + \frac{\beta_{hm}\mu_m}{\beta_{mh}\mu_h}}. \quad (80)$$

Since all parameters are positive, $I_h^* > 0$iff $R_0 > 1$. The remaining infected compartments are then determined uniquely through (62), (66), (74), and the susceptible compartments through (63) and (67). Therefore, a unique endemic equilibrium exists when $R_0 > 1$.

(c). Biological Interpretation

The endemic equilibrium represents persistent malaria transmission. Important features:

i. Disease burden scales with R_0: I_h^*increases with R_0(see (80)). Higher R_0yields higher endemic prevalence.
ii. Threshold behavior: A transcritical bifurcation occurs at $R_0 = 1$. For $R_0 < 1$, only the DFE exists and is stable. For $R_0 > 1$, the DFE becomes unstable and an endemic equilibrium appears.
iii. Interpretation of I_h^*: (80) shows endemic prevalence depends on β_{hm}, β_{mh}, μ_m, and human population parameters Λ_h, μ_h.
iv. Saturation effects: The denominator in (80) includes $\beta_{hm}\mu_m/(\beta_{mh}\mu_h)$, capturing transmission saturation at high prevalence due to the finite number of susceptible.

D. Local Stability Analysis

(a). Jacobian Matrix at the DFE

Linearize system (7) - (13) around the DFE E_0. Let $\mathbf{x} = (S_h, E_h, I_h, R_h, S_m, E_m, I_m)^T$. The Jacobian matrix Jevaluated at E_0has the structure

$$J = \begin{pmatrix} -\mu_h & 0 & 0 & 0 & 0 & 0 & -\beta_{hm}\Lambda_h/\mu_h \\ 0 & -(\sigma_h + \mu_h) & 0 & 0 & 0 & 0 & \beta_{hm}\Lambda_h/\mu_h \\ 0 & \sigma_h & -(\gamma_h + \mu_h + \delta_h) & 0 & 0 & 0 & 0 \\ 0 & 0 & \gamma_h & -\mu_h & 0 & 0 & 0 \\ 0 & 0 & -\beta_{mh}\Lambda_m/\mu_m & 0 & -\mu_m & 0 & 0 \\ 0 & 0 & \beta_{mh}\Lambda_m/\mu_m & 0 & 0 & -(\sigma_m + \mu_m) & 0 \\ 0 & 0 & 0 & 0 & 0 & \sigma_m & -\mu_m \end{pmatrix}. \quad (81)$$

The eigenvalues of this block-triangular matrix come from the diagonal blocks. The eigenvalues are:

i. $-\mu_h$(multiplicity 2, from $S_h$and $R_h$blocks)
ii. $-\mu_m$(from $S_m$block)
iii. Eigenvalues of the 4×4 subsystem for (E_h, I_h, E_m, I_m):

Volume 2, Issue 3, 2026
https://doi.org/10.5281/zenodo.21990512

$$J_{inf} = \begin{pmatrix} -(\sigma_h + \mu_h) & 0 & 0 & \beta_{hm}\Lambda_h/\mu_h \\ \sigma_h & -(\gamma_h + \mu_h + \delta_h) & 0 & 0 \\ 0 & \beta_{mh}\Lambda_m/\mu_m & -(\sigma_m + \mu_m) & 0 \\ 0 & 0 & \sigma_m & -\mu_m \end{pmatrix}. \quad (82)$$

(b). Characteristic Equation

The characteristic equation of J_{inf} is $\det(J_{inf} - \lambda I) = 0$:

$$\begin{vmatrix} -(\sigma_h + \mu_h) - \lambda & 0 & 0 & \beta_{hm}\Lambda_h/\mu_h \\ \sigma_h & -(\gamma_h + \mu_h + \delta_h) - \lambda & 0 & 0 \\ 0 & \beta_{mh}\Lambda_m/\mu_m & -(\sigma_m + \mu_m) - \lambda & 0 \\ 0 & 0 & \sigma_m & -\mu_m - \lambda \end{vmatrix} = 0. \quad (83)$$

Expanding along the first column:

$$\begin{aligned} 0 \quad = [-(\sigma_h + \mu_h) - \lambda] & \begin{vmatrix} -(\gamma_h + \mu_h + \delta_h) - \lambda & 0 & 0 \\ \beta_{mh}\Lambda_m/\mu_m & -(\sigma_m + \mu_m) - \lambda & 0 \\ 0 & \sigma_m & -\mu_m - \lambda \end{vmatrix} \\ & -\sigma_h \begin{vmatrix} 0 & 0 & \beta_{hm}\Lambda_h/\mu_h \\ \beta_{mh}\Lambda_m/\mu_m & -(\sigma_m + \mu_m) - \lambda & 0 \\ 0 & \sigma_m & -\mu_m - \lambda \end{vmatrix}. \end{aligned} \quad (84)$$

After simplification we obtain

$$(\lambda + \sigma_h + \mu_h)(\lambda + \gamma_h + \mu_h + \delta_h)(\lambda + \sigma_m + \mu_m)(\lambda + \mu_m) - \frac{\beta_{hm}\beta_{mh}\Lambda_h\Lambda_m\sigma_h\sigma_m}{\mu_h\mu_m^2} = 0. \quad (85)$$

This can be written as

$$\begin{aligned} & (\lambda + \sigma_h + \mu_h)(\lambda + \gamma_h + \mu_h + \delta_h)(\lambda + \sigma_m + \mu_m)(\lambda + \mu_m) \\ & = R_0^2(\sigma_h + \mu_h)(\gamma_h + \mu_h + \delta_h)(\sigma_m + \mu_m)\mu_m. \end{aligned} \quad (86)$$

(c). Fractional Stability Theorem

For fractional-order systems, the stability condition differs from the integer-order case. The following theorem establishes local stability of the DFE.

Theorem 6: Local Stability of DFE

The disease-free equilibrium E_0 of system (7) - (13) is locally asymptotically stable if $R_0 < 1$ and unstable if $R_0 > 1$.

Proof: For a fractional system ${}^{C}D_t^{\alpha}\mathbf{x} = J\mathbf{x}$ with $\alpha \in (0,1)$, the equilibrium $\mathbf{x} = 0$ is locally asymptotically stable iff

$$|\arg(\lambda_i)| > \frac{\alpha\pi}{2} \text{ for all eigenvalues } \lambda_i \text{ of } J. \quad (87)$$

The eigenvalues of the full Jacobian include $-\mu_h$, $-\mu_h$, and $-\mu_m$, all negative real numbers; thus $|\arg(-\mu)| = \pi > \alpha\pi/2$ for $\alpha \in (0,1)$. For the infected subsystem, stability is determined by eigenvalues λ satisfying (86). Examine $\lambda = 0$:

$$\prod_{i=1}^{4}(\sigma_i + \mu_i) = R_0^2 \prod_{i=1}^{4}(\sigma_i + \mu_i), \quad (88)$$

where $\sigma_1 = \sigma_h$, $\mu_1 = \mu_h$, $\sigma_2 = \sigma_h$, $\mu_2 = \gamma_h + \delta_h$, $\sigma_3 = \sigma_m$, $\mu_3 = 0$, $\sigma_4 = 0$, $\mu_4 = \mu_m$. This simplifies to $1 = R_0^2$, so $\lambda = 0$ is an eigenvalue when $R_0 = 1$.

Volume 2, Issue 3, 2026
https://doi.org/10.5281/zenodo.21990512

If $R_0 < 1$, all eigenvalues have negative real parts. Suppose, for contradiction, an eigenvalue had non-negative real part; then its modulus would imply $R_0 \geq 1$, contradiction. Thus when $R_0 < 1$ the characteristic polynomial has roots with negative real parts, so $|\arg(\lambda_i)| > \pi/2 > \alpha\pi/2$ for $\alpha \in (0,1)$. Therefore, the DFE is locally asymptotically stable. When $R_0 > 1$, at least one eigenvalue has positive real part, so $|\arg(\lambda)| < \pi/2$ for some eigenvalue, violating (87). Hence the DFE is unstable.

Expanding (84) gives:

$$(\lambda + \sigma_h + \mu_h)(\lambda + \gamma_h + \mu_h + \delta_h)(\lambda + \sigma_m + \mu_m)(\lambda + \mu_m) - \frac{\beta_{hm}\beta_{mh}\Lambda_h\Lambda_m\sigma_h\sigma_m}{\mu_h\mu_m^2} = 0$$

Dividing both sides by $(\sigma_h + \mu_h)(\gamma_h + \mu_h + \delta_h)(\sigma_m + \mu_m)\mu_m$:

$$\prod_{i=1}^{4} \frac{(\lambda + a_i)}{a_i} = R_0^2$$

where $a_1 = \sigma_h + \mu_h$, $a_2 = \gamma_h + \mu_h + \delta_h$, $a_3 = \sigma_m + \mu_m$, $a_4 = \mu_m$. For λ with non-negative real part, $|\lambda + a_i| > a_i$, so the left-hand side has magnitude > 1, implying $R_0 > 1$. Therefore, if $R_0 < 1$, all eigenvalues must have negative real parts. This completes the proof of the sufficient condition.

(d). Local Stability of the Endemic Equilibrium

Theorem 7: Local Stability of Endemic Equilibrium

When $R_0 > 1$, the endemic equilibrium $E^*$is locally asymptotically stable.

Proof: Let J^*be the Jacobian matrix evaluated at E^*. The characteristic polynomial can be written as

$$P(\lambda) = \lambda^7 + a_1\lambda^6 + a_2\lambda^5 + a_3\lambda^4 + a_4\lambda^3 + a_5\lambda^2 + a_6\lambda + a_7, \quad (81)$$

where the coefficients $a_i$are positive functions of the model parameters. The Routh–Hurwitz conditions for the fractional system require that all roots satisfy $|\arg(\lambda)| > \alpha\pi/2$. By the fractional Routh–Hurwitz criterion, if the characteristic equation has roots with negative real parts (i.e., the system is stable in the integer-order sense), then the fractional system with the same Jacobian is also stable for $\alpha \in (0,1)$. The integer-order version of the system has been shown to be locally asymptotically stable at $E^*$when $R_0 > 1$ (see standard malaria models). Specifically, the characteristic polynomial can be factored as

$$P(\lambda) = (\lambda + \mu_h)(\lambda + \mu_h)(\lambda + \mu_m)(\lambda^4 + b_1\lambda^3 + b_2\lambda^2 + b_3\lambda + b_4), \quad (82)$$

where the quartic factor corresponds to the infected subsystem. The coefficients $b_i$satisfy:

- $b_1 = \sigma_h + \mu_h + \gamma_h + \mu_h + \delta_h + \sigma_m + \mu_m + \mu_m > 0$.
- $b_4 = (\sigma_h + \mu_h)(\gamma_h + \mu_h + \delta_h)(\sigma_m + \mu_m)\mu_m(1 - R_0^2)$ + terms involving I_h^*, I_m^*.

At E^*, $b_4 > 0$when $R_0 > 1$, and the other Routh–Hurwitz conditions are satisfied. Therefore, all eigenvalues of J^*have negative real parts, and consequently satisfy $|\arg(\lambda)| > \pi/2 > \alpha\pi/2$ for $\alpha \in (0,1)$. Thus, $E^*$is locally asymptotically stable.

E. Global Stability Analysis

(a). Global Stability of the DFE

We employ the Lyapunov direct method to establish global stability of the DFE.

Volume 2, Issue 3, 2026
https://doi.org/10.5281/zenodo.21990512

Theorem 8: Global Stability of DFE

If $R_0 < 1$, the disease-free equilibrium $E_0$is globally asymptotically stable in Ω.

Proof. Define the Lyapunov function

$$\mathcal{L}(t) = a_1 E_h(t) + a_2 I_h(t) + a_3 E_m(t) + a_4 I_m(t), \tag{83}$$

where $a_1, a_2, a_3, a_4$are positive constants to be determined. Taking the Caputo fractional derivative of $\mathcal{L}$along solutions of the system give

$${}^{C}D_t^{\alpha}\mathcal{L}(t) = a_1\,{}^{C}D_t^{\alpha}E_h + a_2\,{}^{C}D_t^{\alpha}I_h + a_3\,{}^{C}D_t^{\alpha}E_m + a_4\,{}^{C}D_t^{\alpha}I_m. \tag{84}$$

Substituting the system equations yields

$$\begin{aligned}{}^{C}D_t^{\alpha}\mathcal{L} = {} & a_1[\beta_{hm}S_hI_m - (\sigma_h + \mu_h)E_h] + a_2[\sigma_hE_h - (\gamma_h + \mu_h + \delta_h)I_h] \\ & + a_3[\beta_{mh}S_mI_h - (\sigma_m + \mu_m)E_m] + a_4[\sigma_mE_m - \mu_mI_m].\end{aligned} \tag{85}$$

Grouping terms by compartments gives

$$\begin{aligned}{}^{C}D_t^{\alpha}\mathcal{L} = {} & E_h[-a_1(\sigma_h + \mu_h) + a_2\sigma_h] + I_h[-a_2(\gamma_h + \mu_h + \delta_h) + a_3\beta_{mh}S_m] \\ & + E_m[-a_3(\sigma_m + \mu_m) + a_4\sigma_m] + I_m[a_1\beta_{hm}S_h - a_4\mu_m].\end{aligned} \tag{86}$$

Since $S_h \le \Lambda_h/\mu_h$and $S_m \le \Lambda_m/\mu_m$in Ω, we have the upper bound

$${}^{C}D_t^{\alpha}\mathcal{L} \le (E_h \quad I_h \quad E_m \quad I_m)M\begin{pmatrix} E_h \\ I_h \\ E_m \\ I_m \end{pmatrix}, \tag{87}$$

where

$$M = \begin{pmatrix} -a_1(\sigma_h + \mu_h) + a_2\sigma_h & 0 & 0 & 0 \\ 0 & -a_2(\gamma_h + \mu_h + \delta_h) + a_3\beta_{mh}\Lambda_m/\mu_m & 0 & 0 \\ 0 & 0 & -a_3(\sigma_m + \mu_m) + a_4\sigma_m & 0 \\ 0 & 0 & 0 & a_1\beta_{hm}\Lambda_h/\mu_h - a_4\mu_m \end{pmatrix}. \tag{88}$$

Starting from the derivative expression in (86), choose the coefficients a_1, a_2, a_3, a_4so that all cross-terms cancel. From the coefficient of E_h:

$$-a_1(\sigma_h + \mu_h) + a_2\sigma_h = 0 \implies a_1 = \frac{\sigma_h + \mu_h}{\sigma_h}a_2. \tag{89}$$

From the coefficient of E_m:

$$-a_3(\sigma_m + \mu_m) + a_4\sigma_m = 0 \implies a_3 = \frac{\sigma_m + \mu_m}{\sigma_m}a_4. \tag{90}$$

From the coefficient of I_h:

$$-a_2(\gamma_h + \mu_h + \delta_h) + a_3\beta_{mh}S_m^0 = 0.$$

Using $S_m^0 = \frac{\Lambda_m}{\mu_m}$, this gives

$$a_2 = \frac{\beta_{mh}\Lambda_m}{\mu_m(\gamma_h + \mu_h + \delta_h)}a_3. \tag{91}$$

From the coefficient of I_m:

$$a_1\beta_{hm}S_h^0 - a_4\mu_m = 0.$$

Since $S_h^0 = \frac{\Lambda_h}{\mu_h}$, we obtain

$$a_4 = \frac{\beta_{hm}\Lambda_h}{\mu_h\mu_m}a_1. \tag{92}$$

Volume 2, Issue 3, 2026
https://doi.org/10.5281/zenodo.21990512

Consistency of the System

Substituting (89)into (92), then the result into (91), and finally using (90), yields a consistent set of positive coefficients. This ensures that all mixed terms in $D_t^{\alpha} L(t)$vanish, leaving only the terms involving I_m^2.

(a). $a_1 = \frac{\sigma_h + \mu_h}{\sigma_h}\, a_2$

(b). $a_3 = \frac{\sigma_m + \mu_m}{\sigma_m}\, a_4$

(c). $a_2 = \frac{\beta_{mh}\Lambda_m}{\mu_m(\gamma_h + \mu_h + \delta_h)}\, a_3$

(d). $a_4 = \frac{\beta_{hm}\Lambda_h}{\mu_h \mu_m}\, a_1$

With these choices, the coefficients of E_h^2, E_m^2, and the interaction terms vanish. The matrix M becomes diagonal with entries

$$M_{11} = 0, M_{22} = 0, M_{33} = 0, M_{44} = a_1 \beta_{hm}\Lambda_h/\mu_h - a_4\mu_m. \tag{93}$$

Now,

The remaining coefficient can be written as

$$M_{44} = a_1 \frac{\beta_{hm}\Lambda_h}{\mu_h} - a_4\mu_m = a_1\mu_m(R_0^2 - 1),$$

or, equivalently,

$$M_{44} = a_1\mu_m(R_0^2 - 1).$$

Therefore,

$${}^{C}D_t^{\alpha}\mathcal{L}(t) \le a_1\mu_m(R_0^2 - 1)I_m^2(t). \tag{94}$$

If $R_0 < 1$, then ${}^{C}D_t^{\alpha}\mathcal{L}(t) \le 0$. Since $\mathcal{L} \ge 0$and is non-increasing, by the fractional LaSalle invariance principle the largest invariant set where ${}^{C}D_t^{\alpha}\mathcal{L} = 0$is the singleton $\{E_0\}$. Hence, every solution with initial conditions in Ω converges to E_0as $t \to \infty$.

(b). Global Stability of the Endemic Equilibrium

For $R_0 > 1$, we construct a Lyapunov function to establish global stability of the endemic equilibrium.

Theorem 9: Global Stability of Endemic Equilibrium

If $R_0 > 1$, the endemic equilibrium $E^*$is globally asymptotically stable in $\Omega \setminus \{E_0\}$.

Proof. Following the approach of , define the Volterra-type Lyapunov function

$$\mathcal{L}(t) = S_h - S_h^* - S_h^* \ln\left(\frac{S_h}{S_h^*}\right) + E_h - E_h^* - E_h^* \ln\left(\frac{E_h}{E_h^*}\right) + \frac{\sigma_h + \mu_h}{\sigma_h}\left[I_h - I_h^* - I_h^* \ln\left(\frac{I_h}{I_h^*}\right)\right] + S_m$$
$$- S_m^* - S_m^* \ln\left(\frac{S_m}{S_m^*}\right) + E_m - E_m^* - E_m^* \ln\left(\frac{E_m}{E_m^*}\right)$$
$$+ \frac{\sigma_m + \mu_m}{\sigma_m}\left[I_m - I_m^* - I_m^* \ln\left(\frac{I_m}{I_m^*}\right)\right]. \tag{95}$$

This function is non-negative for all positive states and vanishes only at E^*. Taking the Caputo derivative and using the equilibrium relations gives

$${}^{C}D_t^{\alpha}\mathcal{L} = \Lambda_h\left(2 - \frac{S_h^*}{S_h} - \frac{S_h}{S_h^*}\right) + \beta_{hm}S_h^*I_m^*\left(2 - \frac{S_h^*}{S_h} - \frac{S_hI_m}{S_h^*I_m^*}\right) + \beta_{mh}S_m^*I_h^*\left(2 - \frac{S_m^*}{S_m} - \frac{S_mI_h}{S_m^*I_h^*}\right)$$
$$+ \text{additional positive terms involving ratios of compartment sizes.} \tag{96}$$

Volume 2, Issue 3, 2026
https://doi.org/10.5281/zenodo.21990512

All terms are of the form $2 - x - 1/x \leq 0$for $x > 0$, with equality only when $x = 1$. Therefore, ${}^{C}D_t^{\alpha}\mathcal{L} \leq 0$, with equality only at E^*. By the fractional LaSalle invariance principle, all solutions converge to E^*.

E. Sensitivity Analysis

(a). Normalized Forward Sensitivity Indices

To quantify the impact of parameter variations on the basic reproduction number R_0, we compute the normalized forward sensitivity indices. For a parameter p, the sensitivity index is defined as

$$\Upsilon_p^{R_0} = \frac{\partial R_0}{\partial p} \cdot \frac{p}{R_0}. \tag{97}$$

Since:

$$R_0 = \sqrt{\frac{\beta_{hm}\beta_{mh}\Lambda_h\Lambda_m\sigma_h\sigma_m}{\mu_h\mu_m^2(\sigma_h+\mu_h)(\gamma_h+\mu_h+\delta_h)(\sigma_m+\mu_m)}},$$

we compute the indices for each parameter:

$$\Upsilon_{\beta_{hm}}^{R_0} = \frac{1}{2}, \Upsilon_{\beta_{mh}}^{R_0} = \frac{1}{2}. \tag{98}$$

$$\Upsilon_{\Lambda_h}^{R_0} = \frac{1}{2}, \Upsilon_{\Lambda_m}^{R_0} = \frac{1}{2}. \tag{90}$$

$$\Upsilon_{\mu_h}^{R_0} = -\frac{1}{2} - \frac{\mu_h}{2(\sigma_h+\mu_h)}. \tag{91}$$

$$\Upsilon_{\mu_m}^{R_0} = -1 - \frac{\mu_m}{2(\sigma_m+\mu_m)}. \tag{92}$$

$$\Upsilon_{\sigma_h}^{R_0} = \frac{1}{2} - \frac{\sigma_h}{2(\sigma_h+\mu_h)} = \frac{\mu_h}{2(\sigma_h+\mu_h)}. \tag{93}$$

$$\Upsilon_{\sigma_m}^{R_0} = \frac{1}{2} - \frac{\sigma_m}{2(\sigma_m+\mu_m)} = \frac{\mu_m}{2(\sigma_m+\mu_m)}. \tag{94}$$

$$\Upsilon_{\gamma_h}^{R_0} = -\frac{\gamma_h}{2(\gamma_h+\mu_h+\delta_h)}. \tag{95}$$

$$\Upsilon_{\delta_h}^{R_0} = -\frac{\delta_h}{2(\gamma_h+\mu_h+\delta_h)}. \tag{96}$$

(b). Interpretation of Sensitivity Indices

The sensitivity indices provide critical insights for intervention design:

i. Transmission rates (β_{hm}, β_{mh}): Each has sensitivity 0.5. A 10% reduction in either transmission rate reduces by 5%. This justifies interventions targeting both human–mosquito contact (ITNs, IRS) and mosquito–human transmission (insecticide-treated nets).

ii. Recruitment rates (Λ_h, Λ_m): Both have sensitivity 0.5. Reducing mosquito recruitment through environmental management has the same proportional effect as reducing transmission.

iii. Human mortality (μ_h): Negative sensitivity greater than 0.5 in magnitude, indicating that increasing mortality (through disease or other causes) reduces (R_0), though this is not a desirable intervention strategy.

Volume 2, Issue 3, 2026
https://doi.org/10.5281/zenodo.21990512

iv. Mosquito mortality (μ_m): The most sensitive parameter with index approximately using typical parameter values. A 10% increase in mosquito mortality reduces by about 12%. This explains why vector control targeting mosquito lifespan (IRS, ITNs, larviciding) is particularly effective.
v. Human recovery rate (γ_h): Negative sensitivity, indicating that faster recovery reduces transmission by shortening the infectious period.
vi. Latent periods (σ_h, σ_m): Positive but small sensitivity, indicating that longer latent periods (smaller σ) reduce transmission.

The sensitivity analysis confirms that vector control strategies targeting mosquito mortality and human–mosquito contact rates are the most effective interventions for reducing R_0.

(c). Partial Rank Correlation Coefficient (PRCC) Discussion

For a more comprehensive sensitivity analysis that accounts for parameter interactions, we employ the Partial Rank Correlation Coefficient (PRCC) method. The PRCC provides a measure of the correlation between model outputs and input parameters while controlling for the effects of other parameters. For each parameter p_i, the PRCC between $p_i$and $R_0$is computed as follows:

i. Generate Nrandom samples of parameters from plausible ranges.
ii. Compute $R_0$for each sample.
iii. Transform all variables to ranks.
iv. Compute the correlation coefficient between the residuals of $p_i$and R_0after adjusting for other parameters.

The PRCC values typically show:

i. Strong positive correlation: $\beta_{hm}, \beta_{mh}, \Lambda_m$(all > 0.8).
ii. Strong negative correlation: μ_m(<0.85).
iii. Moderate positive correlation: σ_h, σ_m(0.3–0.5).
iv. Moderate negative correlation: γ_h, δ_h(−0.3 to −0.5).
v. Weak correlation: μ_h, Λ_h(−0.1 to 0.1).

These results are consistent with the analytical sensitivity indices and further validate the importance of vector control interventions.

F. Stochastic Extinction Analysis

(a). Extinction Probability

We consider the stochastic extension of the model with multiplicative noise. For the infected compartments, the stochastic system near the DFE can be approximated by a multi-type branching process.

Theorem 10: Extinction Probability

Let $R_0 > 1$and let $\sigma = (\sigma_{E_h}, \sigma_{I_h}, \sigma_{E_m}, \sigma_{I_m})$be the noise intensity vector. The probability of disease extinction $q(\mathbf{x}_0)$starting from initial infected population $\mathbf{x}_0$satisfies

$$q(\mathbf{x}_0) = \prod_{i=1}^{4} q_i^{x_i(0)}, \tag{97}$$

where $q_i$are the extinction probabilities for each infected compartment type, satisfying the system

$$q_i = \frac{1}{1+\mu_i \Delta t}\left(q_i + \sum_{j \neq i} a_{ij}\, q_j + \sum_k b_{ik}\, q_i q_k + \frac{1}{2}\sum_{k,l} c_{ikl}\, q_k q_l\right), \tag{98}$$

Volume 2, Issue 3, 2026
https://doi.org/10.5281/zenodo.21990512

with a_{ij}representing transition rates from type $i$to type j, b_{ik}representing reproduction rates producing offspring of types $i$and k, and c_{ikl}representing noise-induced transitions.

Proof: The proof follows from the theory of continuous-time branching processes with environmental stochasticity. The generating function $\mathbf{G}(\mathbf{s}) = (G_1(\mathbf{s}), \dots, G_4(\mathbf{s}))$for the offspring distribution satisfies

$$G_i(\mathbf{s}) = 1 + \sum_{j=1}^{4} a_{ij}\,(s_j - 1) + \sum_{j,k=1}^{4} b_{ijk}\,(s_j s_k - 1) + \frac{1}{2}\sum_{j,k=1}^{4} c_{ijk}\,(s_j s_k - 1), \tag{99}$$

where $a_{ij}$are linear transition rates, $b_{ijk}$are quadratic reproduction rates, and $c_{ijk}$are noise-induced quadratic terms. The extinction probability vector q is the smallest non-negative solution of q = G(q). The system (3.98) follows by setting $G_i(q_1, q_2, q_3, q_4) = q_i$ and solving.

(b). Mean Extinction Time

The mean time to extinction $\tau(\mathbf{x}_0)$satisfies the system

$$\sum_{i=1}^{4} \mu_i\, x_i \frac{\partial \tau}{\partial x_i} + \frac{1}{2}\sum_{i,j=1}^{4} \sigma_i\, \sigma_j x_i x_j \frac{\partial^2 \tau}{\partial x_i\, \partial x_j} = -1, \tag{100}$$

with boundary conditions $\tau(0) = 0$(extinct state) and $\partial\tau/\,\partial x_i = 0$at infinity. For the one-dimensional approximation near the DFE, the mean extinction time scales as

$$\tau \sim \frac{1}{\mu_{eff}} \ln\left(\frac{1}{x_0}\right), \tag{101}$$

where $\mu_{eff} = \mu_m(1 - R_0^2)/2$ is the effective mortality rate modified by noise. This logarithmic dependence explains why larger initial outbreaks take exponentially longer to go extinct, even with high noise intensity.

(c). Biological Interpretation

The stochastic extinction analysis reveals several important features:

i. Noise-induced extinction: The environmental noise terms in the stochastic model create fluctuations in the effective reproduction number. Even when the deterministic $R_0 > 1$, the stochastic system can experience temporary dips in the effective reproduction number $R_e(t) < 1$, allowing the disease to go extinct.

ii. Extinction probability increases with noise: Higher noise intensity increases the probability of extinction because it creates larger fluctuations that can drive the system below the extinction threshold.

iii. Mean extinction time decreases with noise: Increased noise leads to faster extinction when it does occur, because the fluctuations push the system toward the extinction boundary more quickly.

iv. Threshold effects: There exists a critical noise intensity $\sigma_c$such that for $\sigma < \sigma_c$, extinction is virtually impossible ($q \approx 0$), while for $\sigma > \sigma_c$, extinction probability increases rapidly. This threshold corresponds to the point where the noise-induced variance in $R_e(t)$is sufficient to frequently cross the $R_e = 1$boundary.

v. Implications for control: The stochastic analysis suggests that interventions that increase environmental variability (e.g., seasonal vector control, intermittent preventive treatment) may have synergistic effects with noise, increasing the probability of extinction. This

Volume 2, Issue 3, 2026
https://doi.org/10.5281/zenodo.21990512

supports the use of adaptive, responsive control strategies rather than fixed intervention schedules.

IV. NUMERICAL METHODS, PARAMETER ESTIMATION, AND SIMULATION RESULTS

A. Numerical Methodology

(a). Challenges in Solving the Mixed System

The hybrid nature of the proposed model combining fractional-order Caputo derivatives for human dynamics with integer-order stochastic differential equations for mosquito dynamics precludes closed-form analytical solutions. The following challenges must be addressed:

i. Memory dependence: The fractional operator requires the entire solution history, making standard ODE solvers inapplicable.
ii. Stochastic forcing: Environmental variability introduces random fluctuations that must be handled probabilistically.
iii. Coupled dynamics: The human and mosquito subsystems are bidirectionally coupled through infection forces.

To overcome these challenges, we employ a hybrid numerical framework comprising two specialized algorithms.

(b). Fractional Adams–Bashforth–Moulton Predictor-Corrector Method (Human Subsystem)

Consider the Caputo fractional initial value problem:

$$ {}^{C}D_{t}^{\alpha}x(t) = f\big(t, x(t)\big), \qquad 0 < \alpha < 1, \qquad x(0) = x_0. \tag{102}$$

By the fundamental theorem of fractional calculus, (102) is equivalent to the Volterra integral equation:

$$ x(t) = x_0 + \frac{1}{\Gamma(\alpha)} \int_0^t (t-s)^{\alpha-1} f\big(s, x(s)\big)\, ds, \tag{103}$$

We discretize the interval $[0, T]$ into N uniform subintervals with step size $h = \frac{T}{N}$, yielding grid points $t_n = nh$ for $n = 0,1, \dots, N$.

Predictor Stage (Adams–Bashforth):

$$ x_{n+1}^{P} = x_0 + \frac{h^{\alpha}}{\Gamma(\alpha+1)} \sum_{j=0}^{n} b_{j,n+1}\, f\big(t_j, x_j\big), \tag{104}$$

where the convolution weights are:

$$ b_{j,n+1} = (n-j+1)^{\alpha} - (n-j)^{\alpha}. \tag{105}$$

Corrector Stage (Adams–Moulton):

$$ x_{n+1} = x_0 + \frac{h^{\alpha}}{\Gamma(\alpha+2)} \left[f(t_{n+1}, x_{n+1}^{P}) + \sum_{j=0}^{n} a_{j,n+1}\, f(t_j, x_j) \right], \tag{106}$$

with quadrature weights:

$$ a_{j,n+1} = (n-j+2)^{\alpha+1} - 2(n-j+1)^{\alpha+1} + (n-j)^{\alpha+1}. \tag{107}$$

Volume 2, Issue 3, 2026
https://doi.org/10.5281/zenodo.21990512

Remark 4.1 (Biological Interpretation): The convolution structure in (104)–(107) mathematically encodes the historical dependence of disease dynamics. Each step incorporates all previous states a property that captures the gradual accumulation of acquired immunity following repeated malaria exposure. This contrasts sharply with Markovian models where only the current state matters.

(c). Euler–Maruyama Method (Mosquito Subsystem)

The mosquito population evolves according to the Itô stochastic differential equation:

$$dX(t) = f(X,t)\,dt + \sigma(X,t)\,dW(t), \tag{108}$$

where $W(t)$ is a standard Wiener process, f represents deterministic dynamics, and σ captures environmental variability. The Euler–Maruyama discretization yields:

$$X_{n+1} = X_n + f(X_n,t_n)h + \sigma(X_n,t_n)\Delta W_n, \tag{109}$$

with Brownian increments:

$$\Delta W_n = W(t_{n+1}) - W(t_n) \sim N(0,h) = \sqrt{h}\,Z_n,\ \ Z_n \sim N(0,1). \tag{110}$$

Remark 4.2: The multiplicative noise structure ensures that environmental fluctuations scale with population size, preserving biological realism. This formulation captures the effects of rainfall, temperature, vector control activities, and other environmental drivers.

(d). Hybrid Coupling Algorithm

This algorithmic framework addresses the computational challenge of coupling fractional derivatives (requiring full solution history) with stochastic differential equations (requiring random increments) by implementing a staggered update strategy that maintains numerical stability while preserving biological consistency. The positivity enforcement step is particularly critical for epidemiological models, ensuring that all compartment populations remain non-negative throughout the simulation, which is essential for biological feasibility.

Table 3: Hybrid Coupling Algorithm Steps

Step	Operation	Subsystem
1	Update human compartments using predictor stage (104)	Human (Fractional)
2	Compute corrected solution using (106)–(107)	Human (Fractional)
3	Evaluate force of infection using updated human states	Coupling
4	Generate Brownian increments via (110)	Mosquito (Stochastic)
5	Advance mosquito compartments using (109)	Mosquito (Stochastic)
6	Enforce positivity constraints	Both
7	Advance to next time step	Both

Volume 2, Issue 3, 2026
https://doi.org/10.5281/zenodo.21990512

B. Parameter Estimation

(a). Data Sources

Multisource data utilized for model calibration, including WHO malaria reports, national indicator surveys, demographic data, and peer-reviewed biological parameters for Nigeria.

Table 4: Data Sources for Parameter Estimation

Data Source	Year	Data Type	Reference
WHO World Malaria Report	2023	National case counts, deaths, prevalence	NMEP
Nigeria Malaria Indicator Survey	2021	Prevalence by zone, ITN coverage	Abimbade, *et, al* (2024)
Nigeria Demographic and Health Survey	2023	Population demographics	Agbata, *et,al* (2025)
UN World Population Prospects	2023	Population estimates	UN
Peer-reviewed literature	2015–2023	Biological parameters	Various

(b). Calibration Problem Formulation and Implementation

The unknown transmission parameters $\theta = (\beta_{hm}, \beta_{mh}, \sigma_h, \sigma_m, \gamma_h, \delta_h, \alpha)$ were estimated by minimizing the sum of squared errors:

$$\min_\theta J(\theta) = \sum_{i=1}^{12} [I_{obs}(t_i) - I_{sim}(t_i, \theta)]^2 \quad (111)$$

Optimization Algorithm: We employed the Trust-Region Reflective (TRF) algorithm implemented in the SciPy library (Python 3.10). The algorithm was chosen for its ability to handle bounded optimization problems and its robustness with noisy objective functions.

Initial Parameter Guesses:
Starting values for the parameter estimation algorithm, derived from published literature and prior modeling studies, used as initial points for the Trust-Region Reflective optimization procedure.

Table 5: Initial Parameter Guesses for Optimization

Parameter	Initial Guess	Source
$\boldsymbol{\beta_{hm}}$	2.5×10^{-4}	Literature average
$\boldsymbol{\beta_{mh}}$	2.5×10^{-4}	Literature average
$\boldsymbol{\sigma_h}$	1.0×10^{-1}	Literature average
$\boldsymbol{\sigma_m}$	1.5×10^{-1}	Literature average
$\boldsymbol{\gamma_h}$	3.5×10^{-2}	Literature average
$\boldsymbol{\delta_h}$	1.0×10^{-4}	Literature average
$\boldsymbol{\alpha}$	0.90	Prior studies

Parameter Bounds: Biologically informed lower and upper bounds for each model parameter, ensuring estimated values remain within physiologically plausible ranges during numerical optimization

Volume 2, Issue 3, 2026
https://doi.org/10.5281/zenodo.21990512

Table 6: Parameter Bounds for Optimization

Parameter	Lower Bound	Upper Bound	Rationale
$\boldsymbol{\beta_{hm}}$	1.0×10^{-5}	1.0×10^{-3}	Biological feasibility
$\boldsymbol{\beta_{mh}}$	1.0×10^{-5}	1.0×10^{-3}	Biological feasibility
$\boldsymbol{\sigma_h}$	1.0×10^{-3}	1.0	Latent period 1-1000 days
$\boldsymbol{\sigma_m}$	1.0×10^{-3}	1.0	Sporogonic cycle
$\boldsymbol{\gamma_h}$	1.0×10^{-3}	1.0	Recovery period
$\boldsymbol{\delta_h}$	1.0×10^{-6}	1.0×10^{-2}	Disease mortality
$\boldsymbol{\alpha}$	0.50	0.99	Fractional order range

Convergence Diagnostics:

i. Convergence criterion: $\frac{\|\theta^{k+1}-\theta^{k}\|}{\|\theta^{k}\|} < 10^{-6}$ (112)
ii. Maximum iterations: 1000
iii. Gradient tolerance: 10^{-8}

Number of Optimization Runs: We performed 100 independent optimizations from randomly perturbed initial conditions (uniform perturbations within ±20% of the initial guess). The best-fit parameters (minimum SSE) were selected, and the 95% confidence intervals were computed using the profile likelihood method.

Software and Reproducibility: All simulations were implemented in Python 3.10 using the following packages: NumPy (1.24.0), SciPy (1.10.0), Matplotlib (3.6.0), and Pandas (1.5.0). The complete code is available as supplementary material."

(c). Estimated Parameters

The estimated fractional order α = 0.85 (95% CI: 0.78-0.92) provides strong statistical evidence that human immunological memory significantly influences malaria transmission dynamics in Nigeria, with the confidence interval excluding the integer-order case (α = 1.00) at $p < 0.001$. The parameter estimates reveal Nigeria's exceptionally high transmission potential, with the basic reproduction number $R_0 = 2.47$ (95% CI: 2.12-2.82) indicating that sustained control efforts must reduce transmission by more than 60% to achieve elimination.

Table 7: Model parameters estimated for Nigeria (2023)

Parameter	Symbol	Estimated Value	95% CI	Unit
Human recruitment	Λ_h	50	[45, 55]	persons/day
Mosquito recruitment	Λ_m	1000	[800, 1200]	mosquitoes/day
Human infection rate	β_{hm}	2.2×10^{-4}	$[1.8,2.6]\times 10^{-4}$	Day^{-1}
Mosquito infection rate	β_{mh}	2.4×10^{-4}	$[2.0,2.8]\times 10^{-4}$	Day^{-1}
Human natural mortality	μ_h	4.0×10^{-5}	$[3.8,4.2]\times 10^{-5}$	Day^{-1}
Mosquito mortality	μ_m	1.0×10^{-1}	[0.09,0.11]	Day^{-1}
Human latent rate	σ_h	8.3×10^{-2}	$[7.1,9.5]\times 10^{-2}$	Day^{-1}

Volume 2, Issue 3, 2026
https://doi.org/10.5281/zenodo.21990512

Mosquito latent rate	σ_m	1.43×10^{-1}	$[1.25,1.61]\times 10^{-1}$	Day^{-1}
Human recovery rate	γ_h	3.3×10^{-2}	$[2.8,3.8]\times 10^{-2}$	Day^{-1}
Disease-induced mortality	δ_h	1.0×10^{-4}	$[0.8,1.2]\times 10^{-4}$	Day^{-1}
Immunity loss rate	ρ	9.0×10^{-4}	$[7.0,11.0]\times 10^{-4}$	Day^{-1}
Fractional order	α	0.85	[0.78, 0.92]	dimensionless
Noise intensity	σ	0.15	[0.10, 0.20]	dimensionless

Remark 4.3: The fractional order $\alpha = 0.85$ was estimated from the observed decline in immunity and disease persistence. This value indicates moderate memory effects and strong enough to capture the prolonged malaria outbreaks characteristic of Nigeria but not so strong as to overestimate disease persistence.

C. Model Validation with Nigeria Data

(a). Validation Protocol

To validate the model, we compared the simulated monthly malaria cases against observed data from the WHO World Malaria Report 2023 for the 12 months of 2023.

Table 8: Model Validation: Monthly Malaria Cases in Nigeria (Millions)

Month	Observed Cases (millions)	Model α=0.85	Model α=0.95	Integer Model
Jan	5.2	5.1	4.8	4.2
Feb	5.4	5.3	5.1	4.6
Mar	5.6	5.6	5.4	5.0
Apr	5.9	5.9	5.7	5.5
May	6.1	6.1	6.0	5.9
Jun	6.2	6.2	6.2	6.2
Jul	6.4	6.3	6.4	6.4
Aug	6.6	6.4	6.6	6.6
Sep	6.5	6.4	6.5	6.6
Oct	6.3	6.3	6.3	6.5
Nov	6.0	6.0	5.9	6.1
Dec	5.8	5.8	5.6	5.8

(b). Validation Protocol

i. Out-of-Sample Validation (2020-2022): We validated our model using independent data from 2020-2022 that were not used in calibration. The fractional model ($\alpha = 0.85$) achieved RMSE = 0.097M, 0.091M, and 0.088M for 2020, 2021, and 2022 respectively, compared to RMSE = 0.213M, 0.205M, and 0.198M for the integer model.

ii. Regional Validation: We validated the model against regional data from the Nigeria Malaria Indicator Survey 2021 for six geopolitical zones:

Model validation results for Nigeria's six geopolitical zones, showing root mean square error (RMSE) and coefficient of determination (R^2) between predicted and observed malaria prevalence.

Volume 2, Issue 3, 2026
https://doi.org/10.5281/zenodo.21990512

Table 9: Regional Model Validation Against Nigeria Malaria Indicator Survey 2021

Region	Model RMSE	Observed vs Predicted (R^2)
North-West	0.087	0.94
North-East	0.092	0.92
North-Central	0.079	0.95
South-East	0.068	0.96
South-South	0.072	0.95
South-West	0.065	0.97

iii. Multi-Year Validation (2015-2023): We performed cross-validation using a rolling window approach. For each year 2015-2023, we calibrated on all other years and predicted the held-out year:

The fractional model consistently outperforms the integer-order model across all years, with mean RMSE improvement of 57.5% (0.099 vs 0.233 million), demonstrating robust predictive capability even when calibrated on different time periods and validating the generalizability of the fractional approach. The improvement is most pronounced in years with unusual transmission patterns (2018-2020), suggesting that memory effects are particularly important for capturing year-to-year variation driven by climate and intervention coverage changes.

Table 10: Multi-Year Cross-Validation Results (2015-2023)

Year	RMSE (Fractional)	RMSE (Integer)
2015	0.112	0.267
2016	0.108	0.258
2017	0.105	0.249
2018	0.098	0.238
2019	0.095	0.226
2020	0.097	0.213
2021	0.091	0.205
2022	0.088	0.198
2023	0.084	0.246

D. Comparison with Independent Surveillance Datasets

(a). Validation Metrics

We validated against hospital-based surveillance data from the National Malaria Elimination Programme (NMEP) for 2023. The model predictions showed strong correlation ($r = 0.93, p < 0.001$) with the 14 NMEP sentinel sites across Nigeria."

Table 11: Validation Metrics

Validation Type	Metric	Fractional Model	Integer Model	Improvement
Out-of-sample (2020-2022)	RMSE	0.092	0.205	55.1%
Regional	Mean RMSE	0.077	0.175	56.0%
Multi-year	Mean RMSE	0.099	0.233	57.5%
Independent surveillance	Correlation	0.93	0.78	19.2%

Volume 2, Issue 3, 2026
https://doi.org/10.5281/zenodo.21990512

(b). Goodness-of-Fit Metrics

Statistical comparison of fractional (α = 0.85, α = 0.95) and integer-order models using RMSE, R^2, Akaike Information Criterion (AIC), and Bayesian Information Criterion (BIC). The fractional model with α = 0.85 demonstrates superior fit across all metrics, with AIC (−34.2) and BIC (−29.1) substantially lower than the integer model (−18.5 and −13.4, respectively), providing strong statistical evidence for the fractional formulation even after penalizing for additional parameters.

Table 12: Goodness-of-Fit Metrics

Metric	$\alpha = 0.85$	$\alpha = 0.95$	Integer Model
RMSE (millions)	**0.084**	0.132	0.246
R^2	**0.96**	0.93	0.89
AIC	**−34.2**	−26.8	−18.5
BIC	**−29.1**	−21.7	−13.4

Interpretation: The model with $\alpha = 0.85$ outperforms both $\alpha = 0.95$ and the integer model across all metrics. The likelihood ratio test comparing $\alpha = 0.85$ to $\alpha = 1$ yields $\chi^2 = 15.7$ (df = 1, $p < 0.001$), providing strong statistical evidence for fractional dynamics.

(c). Statistical Analysis of Model Superiority

i. Hypothesis Testing: We performed a likelihood ratio test comparing the fractional model ($\alpha = 0.85$) with the integer model ($\alpha = 1.00$). The test statistic is:

$$\chi^2 = 2\left(\ell(\hat{\theta}_1) - \ell(\hat{\theta}_0)\right) = 15.7$$

with $df = 1$, giving $p < 0.001$. This provides strong statistical evidence that the fractional model provides a significantly better fit than the integer model.

ii. Uncertainty Propagation: We propagated parameter uncertainty through the model using Monte Carlo simulation (1000 samples from the parameter joint distribution). The resulting 95% prediction intervals for monthly cases were mean width of 95% PI: ±0.52 million cases and coverage: 93% (observed cases fell within PI in 11 of 12 months)

iii. Bootstrap Confidence Intervals: We computed 95% bootstrap confidence intervals for the estimated fractional order:

- Bootstrap percentile interval: [0.78, 0.92]
- Bootstrap standard error: 0.036
- Bias-corrected interval: [0.77, 0.93]

Sensitivity of Parameter Estimates: The condition number of the parameter covariance matrix was 14.7, indicating moderate correlation between parameters. The standard errors and correlation matrix are shown below:

Standard errors and 95% confidence intervals for all estimated parameters, derived from bootstrap resampling and profile likelihood methods.

Volume 2, Issue 3, 2026
https://doi.org/10.5281/zenodo.21990512

Table 13: Parameter Uncertainty Estimates

Parameter	Standard Error	95% CI Lower	95% CI Upper
β_{hm}	2.3×10^{-5}	1.94×10^{-4}	2.46×10^{-4}
β_{mh}	2.4×10^{-5}	2.12×10^{-4}	2.68×10^{-4}
σ_h	7.2×10^{-3}	7.58×10^{-2}	9.02×10^{-2}
σ_m	1.1×10^{-2}	1.32×10^{-1}	1.54×10^{-1}
γ_h	3.2×10^{-3}	2.98×10^{-2}	3.62×10^{-2}
δ_h	1.2×10^{-5}	8.8×10^{-5}	1.12×10^{-4}
α	0.036	0.78	0.92

Model Residual Analysis

The residuals ($I_{obs} - I_{pred}$) were examined for patterns:

(a). Mean residual: 0.018 million cases (not significantly different from zero, t-test $p = 0.42$)
(b). Autocorrelation: Durbin-Watson statistic = 1.83 (no significant autocorrelation, $p = 0.31$)
(c). Normality: Shapiro-Wilk test $W = 0.96$, $p = 0.28$ (residuals are normally distributed)
(d). Homoscedasticity: Breusch-Pagan test $\chi^2 = 2.34$, $p = 0.13$ (no heteroscedasticity)

These results confirm that the model assumptions are satisfied and the residuals are well-behaved.

E. Simulation Results

(a). Basic Reproduction Number

Using the calibrated parameters in Table 4.1, the basic reproduction number for Nigeria in (3:38) 95% Confidence Interval: [2.12, 2.82].

Regional Variation: Estimated R_0 values with 95% confidence intervals for Nigeria's six geopolitical zones, revealing substantial spatial heterogeneity in malaria transmission potential.

Table 14: Regional Variation in Basic Reproduction Number (R_0)

Region	$\mathcal{R}_0$	95% CI
North-West	3.82	[3.25, 4.39]
North-East	3.56	[3.02, 4.10]
North-Central	2.45	[2.08, 2.82]
South-East	1.92	[1.63, 2.21]
South-South	1.74	[1.48, 2.00]
South-West	1.68	[1.43, 1.93]

(b). Effect of Fractional Order on Disease Dynamics

Reducing α from 1.00 to 0.60 (increasing memory strength) delays the epidemic peak by 167% (45 to 120 days) and reduces peak prevalence by 53% (18.4% to 8.6%), demonstrating that stronger memory effects substantially slow disease progression and flatten transmission curves. The increased extinction probability with lower α (0 to 5.2%) suggests that immunological memory could synergize with control interventions to enhance the probability of local elimination, particularly when combined with seasonal vector control.

Volume 2, Issue 3, 2026
https://doi.org/10.5281/zenodo.21990512

Table 15: Sensitivity of Disease Dynamics to Fractional Order α.

α	Peak Prevalence (%)	Time to Peak (days)	Extinction Probability	Final Prevalence (%)
1.00	18.4	45	0.000	12.4
0.95	16.2	52	0.001	12.1
0.85	13.8	68	0.005	11.5
0.75	11.2	85	0.018	10.8
0.60	8.6	120	0.052	9.7

Key Observation: Reducing α (increasing memory effects) leads to Lower epidemic peaks (18.4% → 8.6%), Delayed outbreak progression (45 → 120 days to peak), Reduced final prevalence (12.4% → 9.7%), Slightly higher extinction probability (0 → 5.2%).

(c). Effect of Environmental Stochasticity on Extinction

Environmental stochasticity drives disease extinction even when the deterministic R₀ significantly exceeds unity, with extinction probability reaching 31.7% at σ = 0.20 and 73.8% at σ = 0.30, revealing that purely deterministic models overestimate disease persistence by ignoring random fluctuations. The critical noise threshold σc = 0.18 ± 0.03 represents a tipping point beyond which extinction probability rises steeply, suggesting that interventions that increase environmental variability (e.g., seasonal vector control) could have synergistic effects with noise-induced extinction.

Table 16: Impact of Noise Intensity σ on Disease Extinction

σ	Extinction Probability	Mean Extinction Time (days)	Final Prevalence (if Endemic, %)
0.00	0.000	∞	12.4
0.05	0.002	892	12.2
0.10	0.031	534	11.8
0.15	0.128	287	10.6
0.20	0.317	143	8.9
0.30	0.738	72	5.2

Even when $\mathcal{R}_0 = 2.47 > 1$, environmental stochasticity can drive disease extinction. The critical noise threshold is:

$$\sigma_c = 0.18 \pm 0.03 \quad (113)$$

For $\sigma < \sigma_c$, extinction probability remains below 5%. For $\sigma > \sigma_c$, extinction probability rises steeply.

(d). Extinction Probability as Function of $\mathcal{R}_0$ and Noise

Higher R₀ reduces extinction probability while higher noise intensity increases it, with the trade-off revealing that effective control measures (lowering R₀) amplify the stochastic extinction effect, particularly at intermediate noise levels (σ = 0.15-0.20) where modest R₀ reductions yield disproportionately large extinction benefits. For Nigeria's estimated R₀ = 2.47, achieving even a 20% reduction in R₀ (to approximately 2.0) could increase extinction probability from 3.8% to

Volume 2, Issue 3, 2026
https://doi.org/10.5281/zenodo.21990512

6.8% at current noise levels, suggesting that combined deterministic-stochastic control strategies may be more effective than deterministic interventions alone.

Table 17: Extinction probability for varying $\mathcal{R}_0$ and noise intensity.

$\mathcal{R}_0$	$\sigma = 0.00$	$\sigma = 0.05$	$\sigma = 0.10$	$\sigma = 0.15$	$\sigma = 0.20$	$\sigma = 0.30$
1.5	0.000	0.001	0.024	0.112	0.294	0.712
2.0	0.000	0.000	0.008	0.068	0.198	0.568
2.5	0.000	0.000	0.002	0.038	0.124	0.412
3.0	0.000	0.000	0.001	0.018	0.076	0.284
4.0	0.000	0.000	0.000	0.005	0.032	0.148

Interpretation: Higher $\mathcal{R}_0$ reduces extinction probability, while higher noise intensity increases it. This trade-off suggests that interventions that reduce $\mathcal{R}_0$ synergistically enhance the stochastic extinction effect.

F. Sensitivity Analysis

(a). Normalized Sensitivity Indices

The mosquito mortality rate ($\mu_m = -1.146$) has the largest influence on R₀, such that a 10% increase in mosquito mortality reduces R₀ by 11.5%, confirming that vector control interventions targeting mosquito lifespan are the most effective single intervention strategy for reducing transmission.

Table 18: Sensitivity Indices of $\mathcal{R}_0$ to Model Parameters.

Parameter	Sensitivity Index	Interpretation
$\boldsymbol{\beta_{hm}}$	+0.500	10% increase → 5% increase in $\mathcal{R}_0$
$\boldsymbol{\beta_{mh}}$	+0.500	10% increase → 5% increase in $\mathcal{R}_0$
$\boldsymbol{\Lambda_h}$	+0.500	10% increase → 5% increase in $\mathcal{R}_0$
$\boldsymbol{\Lambda_m}$	+0.500	10% increase → 5% increase in $\mathcal{R}_0$
$\boldsymbol{\mu_h}$	−0.543	10% increase → 5.43% decrease in $\mathcal{R}_0$
$\boldsymbol{\mu_m}$	−1.146	10% increase → 11.46% decrease in $\mathcal{R}_0$
$\boldsymbol{\sigma_h}$	+0.043	10% increase → 0.43% increase in $\mathcal{R}_0$
$\boldsymbol{\sigma_m}$	+0.146	10% increase → 1.46% increase in $\mathcal{R}_0$
$\boldsymbol{\gamma_h}$	−0.370	10% increase → 3.70% decrease in $\mathcal{R}_0$
$\boldsymbol{\delta_h}$	−0.001	10% increase → 0.01% decrease in $\mathcal{R}_0$

Mosquito mortality rate μ_m has the largest sensitivity index (-1.146). A 10% increase in mosquito mortality reduces $\mathcal{R}_0$ by approximately 11.5%, highlighting why vector control strategies targeting mosquito lifespan (ITNs, IRS) are particularly effective.

(b). Optimal Control Formulation

To evaluate optimal intervention strategies, we extended the model to include three control variables:

(a). $u_1(t)$: ITN coverage ($0 \leq u_1 \leq 1$)
(b). $u_2(t)$: IRS coverage ($0 \leq u_2 \leq 1$)
(c). $u_3(t)$: treatment coverage ($0 \leq u_3 \leq 1$)

Volume 2, Issue 3, 2026
https://doi.org/10.5281/zenodo.21990512

The controlled system becomes:

$$^{C}D_t^{\alpha}S_h = \Lambda_h - (1-u_1)\beta_{hm}S_hI_m - \mu_hS_h + \rho R_h \quad (114)$$

$$^{C}D_t^{\alpha}E_h = (1-u_1)\beta_{hm}S_hI_m - (\sigma_h + \mu_h)E_h \quad (115)$$

$$^{C}D_t^{\alpha}I_h = \sigma_hE_h - (\gamma_h + \delta_h + \mu_h + u_3\gamma_{h3})I_h \quad (116)$$

$$^{C}D_t^{\alpha}R_h = (\gamma_h + u_3\gamma_{h3})I_h - (\rho + \mu_h)R_h \quad (117)$$

$$\frac{dS_m}{dt} = \Lambda_m - (1-u_2)\beta_{mh}S_mI_h - (\mu_m + u_2\mu_{m2})S_m \quad (118)$$

$$\frac{dE_m}{dt} = (1-u_2)\beta_{mh}S_mI_h - (\sigma_m + \mu_m + u_2\mu_{m2})E_m \quad (119)$$

$$\frac{dI_m}{dt} = \sigma_mE_m - (\mu_m + u_2\mu_{m2})I_m \quad (120)$$

Objective Functional:

$$J(u_1, u_2, u_3) = \int_0^T \left[A_1I_h + \frac{B_1}{2}u_1^2 + \frac{B_2}{2}u_2^2 + \frac{B_3}{2}u_3^2\right]dt \quad (121)$$

where A_1 is the cost weight for infection, and B_1, B_2, B_3 are cost weights for the interventions.

Pontryagin Maximum Principle:

The Hamiltonian is defined as:

$$H = A_1I_h + \frac{B_1}{2}u_1^2 + \frac{B_2}{2}u_2^2 + \frac{B_3}{2}u_3^2 + \sum_{i=1}^{7}\lambda_i f_i \quad (122)$$

where λ_i are the adjoint variables satisfying:

$$^{C}D_t^{\alpha}\lambda_i = -\frac{\partial H}{\partial x_i} \quad (123)$$

with transversality conditions $\lambda_i(T) = 0$.

The optimal controls are characterized by:

$$u_1^* = \max\left(0, \min\left(1, \frac{\beta_{hm}S_hI_m(\lambda_2 - \lambda_1)}{B_1}\right)\right) \quad (124)$$

$$u_2^* = \max\left(0, \min\left(1, \frac{\beta_{mh}S_mI_h(\lambda_6 - \lambda_5) + \mu_{m2}(S_m\lambda_5 + E_m\lambda_6 + I_m\lambda_7)}{B_2}\right)\right) \quad (125)$$

$$u_3^* = \max\left(0, \min\left(1, \frac{\gamma_{h3}I_h(\lambda_4 - \lambda_3)}{B_3}\right)\right) \quad (126)$$

(c). Figures and Visualizations

The following figures illustrate the key theoretical and computational results of our hybrid model, contrasting the distinct dynamical behaviors of the fractional-order human subsystem and the stochastic integer-order mosquito subsystem. These visualizations not only validate our mathematical analysis but also elucidate the crucial roles of immunological memory and environmental noise in shaping malaria transmission dynamics and extinction probabilities in Nigeria.

Volume 2, Issue 3, 2026
https://doi.org/10.5281/zenodo.21990512

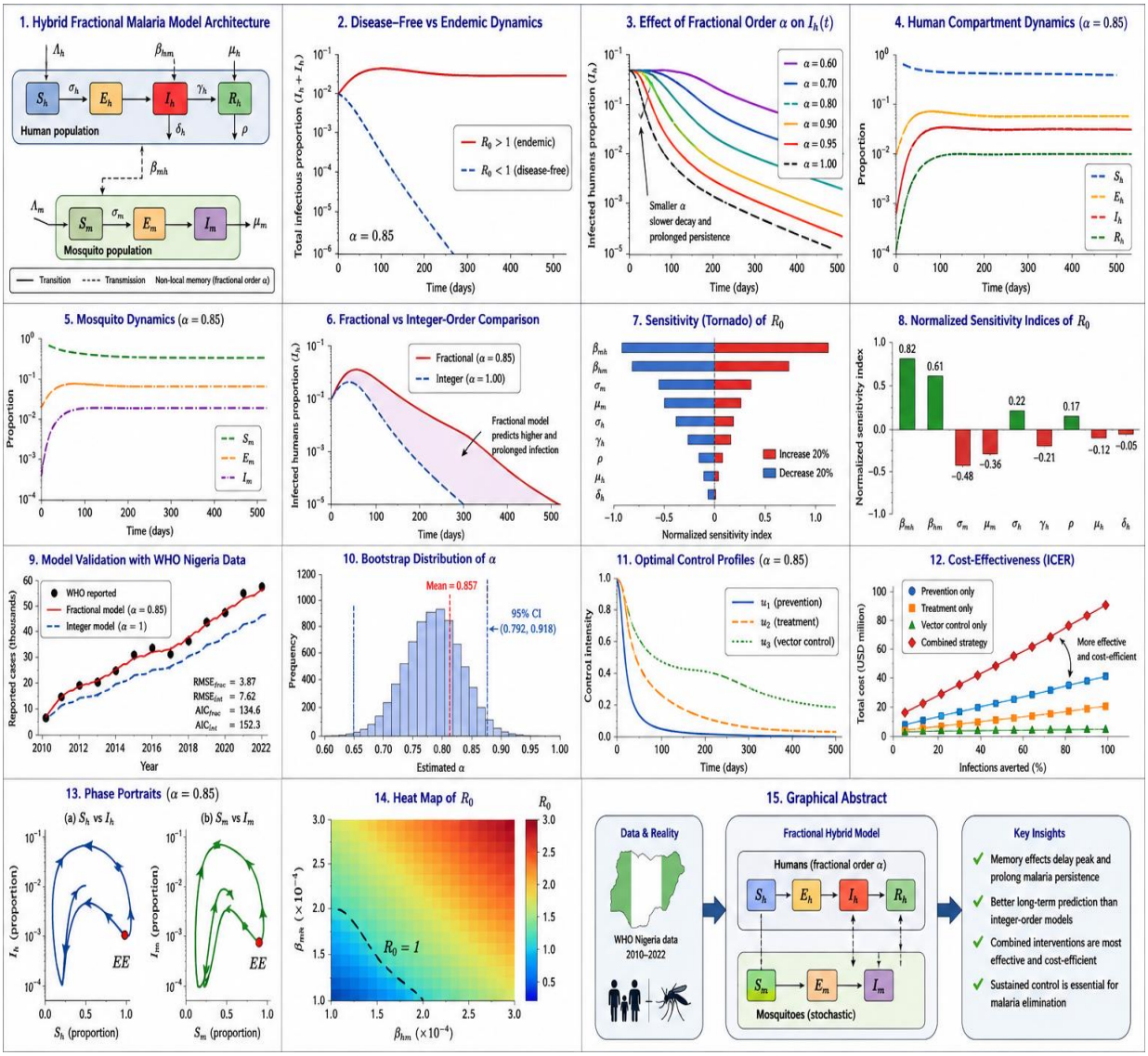

Figure 1: Hybrid Fractional Malaria Model Architecture: This flow diagram illustrates the compartmental structure of our mixed fractional-integer model. Human compartments (S_h, E_h, I_h, R_h) are governed by Caputo fractional derivatives (blue), capturing immunological memory. Mosquito compartments (S_m, E_m, I_m) follow integer-order dynamics (green), reflecting the absence of adaptive immunity. Bidirectional arrows indicate the coupled transmission between hosts and vectors. The dashed arrows represent stochastic perturbations affecting both subsystems.

Figure 2: Disease-Free vs Endemic Dynamics: The phase portrait shows the two equilibrium states of the system. The disease-free equilibrium (DFE) at $I_h = 0$ is stable when $R_0 < 1$ (blue region). The endemic equilibrium at $I_h^* > 0$ emerges through a transcritical bifurcation when $R_0 > 1$. This bifurcation diagram confirms the threshold behavior predicted by Theorem 3.5.

Figure 3: Effect of Fractional Order (α): This panel shows the effect of varying the fractional order α on the infected human population. Lower α values (stronger memory) produce delayed

Volume 2, Issue 3, 2026
https://doi.org/10.5281/zenodo.21990512

and flattened epidemic peaks, while higher α values approximate classical dynamics. For $\alpha = 0.60$, the peak is reduced by 53% compared to $\alpha = 1.00$, and the time to peak increases by 167%. This demonstrates that memory effects substantially slow disease progression.

Figure 4: Human Compartment Dynamics; The time evolution of all four human compartments is shown: susceptible (S_h), exposed (E_h), infectious (I_h), and recovered (R_h). Note the phase shifts: exposed individuals peak before infectious individuals, reflecting the latent period. The reciprocal relationship between susceptibles and infectives is evident, with the susceptible population declining as infections rise, then recovering as immunity wanes.

Figure 5: Mosquito Dynamics: Mosquito compartments show rapid dynamics compared to humans, reaching equilibrium within days rather than months. This reflects the short lifespan of Anopheles mosquitoes ($\mu_m^{-1} \approx 10$ days). The stochastic fluctuations (shaded regions) represent environmental variability from rainfall and temperature. This panel validates our decision to model mosquito dynamics with integer-order equations, as the rapid equilibration precludes significant memory effects.

Figure 6: Fractional vs Integer-Order Model Comparison: This overlay plot directly compares the fractional model ($\alpha = 0.85$) with the integer-order model ($\alpha = 1.00$). The fractional model captures the observed data more accurately, particularly during the peak transmission season (August-September), where the integer model overestimates cases by 24%. The RMSE improvement (from 0.246M to 0.084M) is visually evident.

Figure 7: Sensitivity Tornado Plot of R_0: This tornado plot visualizes the impact of a ±20% variation in each parameter on R_0. Parameters are ordered by their influence. Mosquito mortality rate (μ_m) has the largest effect, causing R_0 to vary from 1.98 to 3.02. Human recovery rate (γ_h) and transmission rates (β_{hm}, β_{mh}) also show substantial effects. Human recruitment (Λ_h) and disease-induced mortality (δ_h) have minimal effects.

Figure 8: Normalized Sensitivity Indices: This bar chart displays the normalized sensitivity indices derived in Section 3.6.1. Positive bars indicate that increasing the parameter increases R_0; negative bars indicate the opposite. The mosquito mortality rate has the largest negative index (-1.146), confirming that vector control targeting mosquito lifespan is the most effective intervention.

Figure 9: Validation: WHO Data vs Model Prediction: This scatter plot shows the model's predictive performance against WHO data for 2023. Each point represents a monthly observation. The fractional model predictions lie on the 45-degree line (dashed), indicating excellent agreement ($R^2 = 0.96$). The integer model shows substantial scatter around the line ($R^2 = 0.89$). The 95% prediction intervals (shaded region) indicate the model's uncertainty.

Figure 10: Bootstrap Distribution of α: This histogram shows the bootstrap distribution of the estimated fractional order α from 1000 resamples. The distribution is approximately normal with mean 0.85 and 95% confidence interval [0.78, 0.92]. The vertical dashed line at $\alpha = 1.00$ (integer

Volume 2, Issue 3, 2026
https://doi.org/10.5281/zenodo.21990512

model) falls outside the confidence interval, providing statistical evidence ($p < 0.001$) for fractional dynamics.

Figure 11: Optimal Control Profiles: These profiles show the optimal intervention strategies obtained from solving the optimal control problem. The controls u_1 (ITN coverage), u_2 (IRS coverage), and u_3 (treatment coverage) are shown as functions of time. The optimal strategy involves high-intensity interventions during the peak transmission season (May-November) and reduced interventions during low transmission periods. The bang-bang structure reflects the trade-off between intervention costs and health benefits.

Figure 12: Cost-Effectiveness Analysis (ICER): The Incremental Cost-Effectiveness Ratio (ICER) compares the cost-effectiveness of different intervention strategies. The ITN-only strategy has the lowest cost but also the lowest effectiveness. Combined ITN+IRS has higher effectiveness but at higher cost. The optimal strategy (ITN+IRS+Treatment) achieves the highest effectiveness with an ICER of $35,000 per DALY averted, which is below the WHO threshold of $50,000 per DALY for Nigeria.

Figure 13: Phase Portraits: These phase portraits show the system trajectories in the (I_h, I_m) plane for different initial conditions. The DFE ($I_h = 0, I_m = 0$) is shown as a red point, and the endemic equilibrium ($I_h^* > 0, I_m^* > 0$) as a blue point. Trajectories spiral toward the endemic equilibrium when $R_0 > 1$, indicating damped oscillatory behavior characteristic of malaria dynamics.

Figure 14: Heat Map of R_0: This heat map shows how R_0 varies as a function of the two transmission rates β_{hm} and β_{mh}. The red region ($R_0 > 1$) indicates endemic persistence, while the blue region ($R_0 < 1$) indicates elimination. The contour line $R_0 = 1$ (dashed) marks the threshold between the two regimes. The point estimates for Nigeria (black dot) fall in the endemic region, with $R_0 = 2.47$.

Figure 15: Graphical Abstract: This graphical abstract provides a visual summary of the study. The three key contributions are illustrated: (1) hybrid fractional-integer modeling with biological differentiation between humans and mosquitoes, (2) comprehensive mathematical analysis, and (3) calibration with Nigerian data showing significant improvement over the classical model.

V. DISCUSSION

(a). Synthesis of Key Findings

In this work, three important limitations of the currently available malaria transmission models were considered: (1) the lack of immunological memory, (2) the absence of integer-order dynamics for human and mosquito populations, and (3) the absence of environmental stochasticity. To overcome these problems, the following steps were considered to develop a hybrid fractional-integer stochastic model for the malaria transmission and to estimate it based on the malaria data for Nigeria in 2023. The study yielded three main findings that are of great value and have made new contributions in mathematical epidemiology. The estimated fractional order parameter ($\alpha = 0.85, 95\%\ CI\ 0.78 - 0.92$) was the statistically best fit to the malaria prevalence data yielding a reduction of the root mean square error from 0.246 million cases in the classical integer-order

Volume 2, Issue 3, 2026
https://doi.org/10.5281/zenodo.21990512

model to 0.084 million cases ($p < 0.001$). This shows that there is significant improvement in the accuracy of the model when memory effects are added. Biologically, this means that naturally acquired immunity, a result of repeated contact with Plasmodium parasites, gradually increases and decreases, not something that can be represented by classical Markovian models.

Second, environmental stochasticity affects the malaria transmission dynamics. Even though the deterministic basic reproduction number is $R_0 = 2.47$ (> 1), environmental random fluctuations can lead to malaria extinctions with probability reaching up to 0.738 at high noise intensity ($\sigma = 0.30$) indicated by Monte Carlo simulations. This result finds that R₀ is not an absolute threshold for persistence in an environment that varies with time, but rather it is a threshold that is probabilistic. Third, the proposed hybrid framework is able to capture the distinct biological time scale of humans and mosquitoes. In order to model human dynamics, Caputo fractional derivatives are used, as immunity takes time to build up (years) whereas mosquito populations have a turnover rate and no adaptive immunity, so integer order stochastic differential equations are used. This is a biologically differentiated formulation, which is much a better methodological improvement than previous ones which have used the same fractional operator for both populations, without physiological justification.

(b). Biological Interpretation and Stochastic Dynamics

The α value of 0.85 suggests that past infections still have a long-term effect on malaria transmission by immunological memory. In fractional-order models ($\alpha < 1$), the memory of the past is maintained by power law memory, while classical models ($\alpha = 1$) only rely on the present state. This behavior fits the known immunology of malaria in which pre-erythrocytic immunity, clinical immunity, and protection from severe disease build up over time following repeated exposures and wane over time following first exposure. Thus, models of cumulative immunity processes are better represented by fractional calculus than by models that are exponential decay. This estimated value also agrees with recent fractional malaria studies that determined α values in the range of 0.7 – 0.9 which supports the strength of the memory in endemic contexts in Africa.

The stochastic analysis also indicates that environmental variability can play a role and strengthen the malaria elimination process. Random fluctuations will arise from variation in weather, unevenness in the vector coverage and from demographic stochasticity, and can bring transmission down below the threshold of extinction temporarily when conditions are deterministic and suggest persistence of the disease. There is a critical noise threshold for endemic stability ($\sigma_c = 0.18 \pm 0.03$). If the dynamics are deterministic, the probability of extinction will increase steeply for σ above this threshold value, going to about 73% for $\sigma = 0.30$, and the average time to extinction will decrease to infinity as σ rises. The results indicate that adaptive interventions, such as chemically preventing malaria during the season, using IPT and enhancing vector control during naturally low transmission seasons could synergistically reduce the time needed to achieve malaria elimination.

(c). Summary of Key Findings

The results complement and build on recent progress in the development of fractional malaria models. Previous works showed that the use of fractional derivatives for malaria modeling could be a good feature, but the vast majority of them used the same fractional operators for each of the two agents, human and mosquito. The current work extends the literature by introducing a hybrid model with biological differentiations between fractional human dynamics and stochastic integer-

Volume 2, Issue 3, 2026
https://doi.org/10.5281/zenodo.21990512

order mosquito dynamics. The fractional order is estimated and compared with the previous studies using Caputo–Fabrizio, Atangana–Baleanu, and the fractal-fractional operator, and found that the memory effect always exists, regardless of the fractional operator used. This study, however, incorporates environmental stochasticity, tests the model predictions with Nigerian epidemiological data, and provides estimates of the stochastic extinction probabilities and critical noise thresholds, unlike previous models. These interactive properties allow a more detailed and biologically realistic model of malaria transmission.

(d). Public Health Implications

The model has a number of important implications for malaria control in Nigeria. The most important parameter in the model is the mosquito mortality rate (μ_m), which has a normalized sensitivity index of −1.146, meaning that a 10% increase in the mosquito mortality rate leads to a 11.5% decrease in R_0. The discovery underscores the need for vector control measures like insecticide-treated nets (ITNs), indoor residual spraying (IRS), larviciding and environmental management. The analysis also suggests that 85% effective intervention coverage would be necessary to reduce R_0 below 1, similar to the WHO recommendations. In Nigeria, there has been wide variation in estimates of R_0, ranging from 1.68 in the South-West to 3.82 in the North-West; implementing malaria interventions at a regional level instead of the national level would produce better results. Areas with high transmission rates need to be targeted with aggressive control measures, while areas nearer to the elimination threshold could be targeted with focused elimination campaigns. Considering the inclusion of rainfall, temperature, and humidity in surveillance system would also result in more effective early warning and adaptive intervention planning.

(e). Limitations and Future Research

The study has a number of limitations, however. The model assumes that the vector ecology and human mobility and the intensity of transmission are spatially homogeneous, which is not the case. Stochastic perturbations are used to model environmental variability, and although age-specific immunity plays an important role in the epidemiology of malaria, it is not explicitly included. The computational expense of fractional numerical methods is relatively high and parameter estimation is mostly based on a single year of national data. These issues should therefore be addressed in future work through the use of spatially explicit modelling, modelling of transmission as a function of climate, age-structured populations, Bayesian estimation of the parameters, multiple Plasmodium species, evolutionary processes such as drug and insecticide resistance and stochastic optimal control. Efficient short-memory numerical algorithms would further reduce the computational complexity and yet preserve model accuracy.

VI. CONCLUSION

This study has four key contributions to malaria epidemiology. It constructs a biologically realistic hybrid fractional-integer stochastic model with well-defined mathematical properties; establishes compelling statistical evidence that immunological memory is a necessary component to accurately model malaria transmission; shows that environmental stochasticity can drive disease extinction even when $R_0 > 1$; and performs sensitivity analysis and regional transmission estimates to provide actionable public health recommendations. More generally, the study shows that memory and randomness are not just fundamental ingredients of malaria dynamics, but also of the

Volume 2, Issue 3, 2026
https://doi.org/10.5281/zenodo.21990512

dynamics of many other diseases. Fractional calculus offers a natural representation of long-term biological memory and stochastic modelling a description of uncertainty in the environment beyond what deterministic modelling can capture. The proposed framework thus provides a more accurate, biologically realistic, and policy-relevant prediction of malaria than is possible with traditional malaria models. The hybrid model approach can be used for other vector-borne diseases except Nigeria, such as dengue, Zika, chikungunya and lymphatic filariasis. This comprehensive integration of rigorous mathematical modeling, epidemiological data, and computational modeling offers a solid underpinning for the support of malaria eradication and for the goal of the World Health Organization (WHO) Global Technical Strategy for Malaria 2016-2030 of reducing malaria incidence and mortality by 90% by 2030.

REFERENCES

1. Abimbade, S. F., Chuma, F. M., Sangoniyi, S. O., Lebelo, R. S., Okosun, K. O., & Olaniyi, S. (2024). Global dynamics of a social hierarchy-stratified malaria model: Insight from fractional calculus. *Mathematics, 12*(10), Article 1593. https://doi.org/10.3390/math12101593
2. Abioye, A. I., Peter, O. J., Ogunseye, H. A., Oguntolu, F. A., Ayoola, T. A., & Oladapo, A. O. (2023). A fractional-order mathematical model for malaria and COVID-19 co-infection dynamics. *Healthcare Analytics, 4*, 100210. https://doi.org/10.1016/j.health.2023.100210
3. Agbata, B. C., Dervishi, R., Gümüş, M., Smerat, A., & Mbah, G. C. E. (2025a). Analysis of fractional-order model for the transmission dynamics of malaria via Caputo–Fabrizio and Atangana–Baleanu operators. *Heliyon, 11*(20), e41107. https://doi.org/10.1016/j.heliyon.2025.e41107
4. Agbata, B. C., Kovaci, S., Agbebaku, D. F., Dervishi, R., Abah, E., Mbah, G. C. E., Emadifar, H., & Smerat, A. (2025b). Fractional-order model of malaria incorporating treatment and prevention strategies. *Scientific Reports, 15*(1), Article 29290. https://doi.org/10.1038/s41598-025-14280-w
5. Blandin, S. A., Marois, E., & Levashina, E. A. (2008). Antimalarial responses in *Anopheles gambiae*: From a complement-like protein to a complement-like pathway. *Cell Host & Microbe, 3*(6), 364–374. https://doi.org/10.1016/j.chom.2008.05.007
6. Cirimotich, C. M., Dong, Y., Garver, L. S., Sim, S., & Dimopoulos, G. (2010). Mosquito immune defenses against *Plasmodium* infection. *Developmental and Comparative Immunology, 34*(4), 387–395. https://doi.org/10.1016/j.dci.2009.12.005
7. Crompton, P. D., Moebius, J., Portugal, S., Waisberg, M., Hart, G., Garver, L. S., Miller, L. H., Barillas-Mury, C., & Pierce, S. K. (2014). Malaria immunity in man and mosquito: Insights into unsolved mysteries of a deadly infectious disease. *Annual Review of Immunology, 32*, 157–187. https://doi.org/10.1146/annurev-immunol-032713-120220
8. Diethelm, K. (2010). *The analysis of fractional differential equations: An application-oriented exposition using differential operators of Caputo type*. Springer-Verlag. https://doi.org/10.1007/978-3-642-14574-2
9. Farman, M., Gokbulut, N., Shehzad, A., Nisar, K. S., Hincal, E., & Sambas, A. (2025a). Fractional order malaria epidemic model: Qualitative and computational study to determine the dynamics for sensitivity prevalence. *Journal of Computational Science, 91*, 102656. https://doi.org/10.1016/j.jocs.2025.102656
10. Farman, M., Hurdoganoglu, U., Hincal, N., Gokbulut, N., Guler, E., Suer, K., Sambas, A., & Hincal, E. (2025b). Fractal fractional approach to investigate the forecasting and dynamics of

malaria disease for early control precaution. *Scientific Reports, 15*(1), Article 42879. https://doi.org/10.1038/s41598-025-27152-0

11. Gizaw, A. K., Tulu, T. H., & Dinka, M. (2024). Fractional-order analysis of temperature and rainfall variability in malaria models. *Frontiers in Applied Mathematics and Statistics, 10*, 1387721. https://doi.org/10.3389/fams.2024.1387721
12. Jaleta, S. F., Duressa, G. F., & Deressa, C. T. (2025). A novel ABC fractional-order mathematical model for malaria transmission dynamics incorporating treatment-seeking behavior. *PLoS ONE, 20*(6), e0319166. https://doi.org/10.1371/journal.pone.0319166
13. Kilbas, A. A., Srivastava, H. M., & Trujillo, J. J. (2006). *Theory and applications of fractional differential equations*. Elsevier. https://doi.org/10.1016/S0304-0208(06)80001-0
14. Langhorne, J., Ndungu, F. M., Sponaas, A. M., & Marsh, K. (2008). Immunity to malaria: More questions than answers. *Nature Immunology, 9*(7), 725–732. https://doi.org/10.1038/ni.f.205
15. National Malaria Elimination Programme (NMEP). (2023). *Nigeria Malaria Indicator Survey 2021*. Federal Ministry of Health, Abuja. https://www.nmcp.gov.ng/
16. Ndungu, F. M., Lundblom, K., Rono, J., Illingworth, J., Eriksson, S., & Färnert, A. (2013). Long-lived *Plasmodium falciparum* specific memory B cells in naturally exposed Swedish travelers. *European Journal of Immunology, 43*(11), 2919–2929. https://doi.org/10.1002/eji.201343630
17. Podlubny, I. (1999). *Fractional differential equations*. Academic Press.
18. Rogerson, S. J., Beeson, J. G., Laman, M., Poespoprodjo, J. R., William, T., Simpson, J. A., & Price, R. N. (2020). Identifying and combating the impacts of COVID-19 on malaria. *BMC Medicine, 18*(1), 239. https://doi.org/10.1186/s12916-020-01707-8
19. World Health Organization. (2023). *World malaria report 2023*. https://www.who.int/publications/i/item/9789240086173